

# CHEMICAL EVOLUTION IN HIERARCHICAL MODELS OF COSMIC STRUCTURE I: CONSTRAINTS ON THE EARLY STELLAR INITIAL MASS FUNCTION

JASON TUMLINSON

Department of Astronomy and Astrophysics, University of Chicago, 5640 S. Ellis Ave., Chicago, IL 60637

*Draft version January 25, 2018*

## ABSTRACT

I present a new Galactic chemical evolution model motivated by and grounded in the hierarchical theory of galaxy formation, as expressed by a halo merger history of the Galaxy. This model accurately reproduces the “metallicity distribution function” (MDF) for Population II stars residing today in the Galactic halo. Model MDFs are calculated for a fiducial Galaxy formation scenario and a range of assumptions about the astrophysics of star formation and chemical enrichment at early times. The observed MDF and the apparent absence of true Population III stars from the halo strongly imply that there is some critical metallicity,  $Z_{crit} \lesssim 10^{-4} Z_{\odot}$ , below which low-mass star formation is inhibited, and perhaps impossible. The observed constraints from the halo MDF, relative metal abundances from extremely metal-poor Galactic halo stars, and the ionizing photon budget needed to reionize the IGM together imply a stellar initial mass function (IMF) that is peaked in the range of massive stars that experience core-collapse supernovae, with mean mass  $\langle M \rangle = 8 - 42 M_{\odot}$ . This mass range is similar to the masses predicted by models of primordial star formation that account for formation feedback. A set of five plausible IMF cases is presented, ranging from broadly peaked with mean mass  $\sim 20 M_{\odot}$ , to narrowly peaked at mean mass  $\sim 70 M_{\odot}$ . These IMF cases cannot be distinguished formally by the available constraints, but the models with lower characteristic mass produce overall better fits to the available data. The model also implies that metal-poor halo stars below  $[\text{Fe}/\text{H}] \lesssim -3$  had only 1 - 10 metal-free stars as their supernova precursors, such that the relative abundances in these halo stars exhibit IMF-weighted averages over the intrinsic yields of the first supernovae. This paper is the first part of a long term project to connect the high-redshift *in situ* indicators of early star formation with the low- $z$ , old remnants of the first stars.

*Subject headings:* galaxies:formation – galaxies:evolution – Galaxy:formation – Galaxy:evolution – stars:abundances – stars:mass function – cosmology:theory

## 1. INTRODUCTION

Interest in the first stars is mounting as the frontiers of formerly disparate fields of observing and theory converge at the end of the cosmological “Dark Ages”. Despite theoretical progress and rapid advances in the discovery of high-redshift galaxies, many questions remain open: What is the first-stars IMF? How long did the epoch of metal-free stars last? Did they contribute much to reionization? Do their remnants include compact objects, and if so, where are they? Theorists approach these problems by running the clock forward in simulations of individual stars and primordial galaxies (Tumlinson & Shull 2000; Bromm & Larson 2004). Observers work backward in time, where the frontier marked by the most distant known galaxy is steadily advancing thanks to the *Hubble Space Telescope* (HST) and large ground-based telescopes and is expected to advance rapidly with the launch of *James Webb Space Telescope* (JWST). The highly interdisciplinary “first stars” field is just beginning to confront observations, in the form of reionization tests with the Gunn-Peterson effect and the *Wilkinson Microwave Anisotropy Probe* (WMAP) and chemical abundances from extremely metal-poor Galactic stars. These indicators have yielded some indirect constraints on the nature of the first stars. In the next few years theory will come into closer contact with high-redshift galaxy surveys, and additional insight will come from the growing numbers of old stars in the Milky Way that reveal the detailed metal yields of early supernovae. But neither

high- $z$  galaxies nor the “second stars” will tell the whole story on their own. The most promising theoretical approach is to connect unique high- $z$  signatures of the first stars *in situ* and the Galactic “fossil record” preserved in the second stellar generation.

Following this approach, this paper advances three main goals:

1. A formalism for connecting Galactic chemical evolution to the theory of galaxy formation, so that different observational data can be integrated together.
3. An empirical method for assessing the duration and intensity of metal-free star formation, to complement and anticipate direct observations, and
2. A framework for relating high-redshift galaxy surveys and spectra to Galactic chemical evolution.

This study extends the approach used by, e.g. Tumlinson, Venkatesan, & Shull (2004, hereafter TVS04), who attempted to constrain the first-stars IMF by combining the *WMAP* constraint on early reionization and the observed metal abundances in metal-poor Population II halo stars. That study argued that the joint constraints were best fitted by a first generation with  $10 - 100 M_{\odot}$ , and not the very massive stars (VMSs;  $M \gtrsim 140 M_{\odot}$ ) motivated by some simulations. TVS04 demonstrates the potential of relating signatures of reionization at high redshift with metal-poor stars in the Galaxy, an approach

that has been called “near-field cosmology” (Freeman & Bland-Hawthorn 2002). This introduction provide some additional motivation in terms of recent theoretical and observational advances.

*Goal 1: Connecting Early Chemical Enrichment to Distant Galaxies.* The first and most fundamental project will complete the theoretical framework needed to connect high- and low- $z$  observations. The major missing piece is a formalism that will follow early chemical enrichment in the proper context of galaxy formation. This framework must relate integrated galaxy properties to the detailed metallicity history of their stellar populations. A hierarchical,  $\Lambda$ CDM-based stochastic treatment is needed because early chemical enrichment may proceed unevenly. The earliest pregalactic dark-matter halos are thought to be too small, with  $\lesssim 10^3 - 10^4 M_\odot$  in stars, to contain a representative sample of stars from the IMF, especially if they are all massive stars. The Press-Schechter theory underlying most semi-analytic models of reionization (e.g., Haiman & Loeb 1997; Venkatesan, Tumlinson, & Shull 2003) and the chemical enrichment of the IGM (Scannapieco et al. 2003) can test a wide range of uncertain astrophysical assumptions, but by itself results in an unsuitably deterministic and uniform treatment of early chemical enrichment because it generally treats alike all halos of equal mass. On the other hand, numerical simulations can follow complicated gas physics in three dimensions, but often lack the mass resolution and speed that is required to realize a wide range of physical assumptions.

A better model would combine these approaches, and follow the stochastic history of stellar populations in semi-analytic models. Such a stochastic semi-analytic treatment (e.g., halo-merger trees; Somerville & Primack 1999) is widely used to study galaxy formation and generally succeeds at reproducing galaxy properties. In broad outline, the halo-merger model will calculate the collapse of baryons into protogalaxies, hierarchical mergers into galaxies, and star formation histories over a range of final ( $z = 0$ ) galaxy masses, given the astrophysical parameters. Stellar evolution and atmosphere models (Tumlinson, Shull, & Venkatesan 2003; hereafter TSV03) and detailed metal yields (Heger & Woosley 2002, hereafter HW02; Umeda & Nomoto 2005) will specify the ionizing photon output and the global chemical evolution of the stars and gas. The resulting model will be capable of predicting both (1) color and metallicity diagnostics and evolution for high- $z$  galaxies for comparison to *HST* and *JWST* data at  $z > 6$ , and (2) a model distribution of metal-poor Galactic stars for comparison to the existing samples (Cayrel et al. 2004; Cohen et al. 2004) and eventually to the thousands of metal-poor halo stars expected from large future surveys (SEGUE, WFMOS). Thus, a single model can test astrophysical assumptions for metallicity evolution and IMF of the first stars against both the high- and low- $z$  data. This approach is new; the necessary level of detail in abundances cannot be captured by numerical simulations, and the galaxy-formation context is missing from conventional chemical evolution models.

*Goal 2: The End of the First Stars Epoch: Transition to Normal Star Formation.* By connecting early galaxy formation to Galactic chemical evolution, the complete framework will enable a new approach to what is per-

haps the thorniest problem about the first stars - how long did they last? The final model will constrain the duration of the first-stars epoch with the number counts and element abundances in the metal-poor stars, by deriving a formation history of metal-free stars consistent with Galactic chemical evolution.

Recent theoretical work has focused on *a priori* estimates of the “critical metallicity”,  $Z_{cr} \sim 10^{-5} - 10^{-3} Z_\odot$  (Schneider et al. 2002; Bromm & Loeb 2003; Santoro & Shull 2005), above which gas can cool and fragment to  $\sim 1 M_\odot$ . Below  $Z_{cr}$  a “top-heavy” IMF is expected, owing to the effective absence of metal-line and dust cooling (Bromm, Coppi, & Larson 2001; Abel, Bryan, & Norman 2002). The time required for a galaxy to achieve this metallicity, by itself or by enrichment from its neighbors, is believed to be 100 - 200 Myr (TVS04), but it is difficult to calculate this time from first principles because a number of poorly-understood processes (e.g., mixing in the interstellar medium, transport of metals across the IGM) influence the result. The proposed galaxy formation model will follow these processes to provide an independent estimate by asking instead when the “second stars” - the Galactic Population II stars - were born. The observed abundances of key elements produced by zero-metallicity stars may be just such a “clock”. Ultimately, halo merger histories calibrated by high- $z$  observations can assign a timeframe to the metal-poor stars based on their levels of enrichment ([Fe/H]) and relative abundances in the context of the global model. The approach of relating all available observational data is motivated by this promise of providing powerful logical connections between all constraints, direct and indirect, present and future.

*Goal 3: Explain the Signatures of Early Reionization and High-redshift Galaxies.* As high- $z$  galaxy searches expand to encompass larger, deeper samples, they will eventually enter the transition period between metal-free and metal-enriched star formation and into the epoch of reionization at  $z \gtrsim 6$ . There are already indications from the cosmic microwave background (CMB) that reionization began earlier and was more extended in time than had been expected on theoretical grounds alone. This early reionization can be explained by a variety of models, but the most commonly cited explanation is that early star formation is unusually efficient at converting stellar mass into ionizing photons (Cen 2003; Haiman & Holder 2003; Ciardi et al. 2003; TVS04). Thus the IMF of early star formation is intimately connected with reionization, and it is worth asking whether the populations that accomplished reionization have left any detectable information in the history of Galactic chemical evolution. TVS04 argued for such a connection, and in favor of mutual constraints on the primordial IMF from reionization and chemical evolution. In addition to developing the basic formalism for goals 1 and 2, this paper carries this effort further toward quantitative constraints.

The need for robust metallicity indicators for early galaxies will soon become acute. The unique signatures of truly metal-free populations are expected to be the high Ly $\alpha$  equivalent width (which may have been detected already at  $z \sim 5$ ; Malhotra & Rhoads 2002) and strong He II  $\lambda 1640$  nebular emission (Tumlinson, Giroux, & Shull 2001); these sensitive indicators of stellar IMF from  $10 - 500 M_\odot$  are also unique to  $Z = 10^{-4} Z_\odot$

(Schaerer 2002; TSV03). As shown by TSV03, the broad-band colors of metal-free stellar clusters are easily confused with more metal-rich populations, so Ly $\alpha$  and He II are likely to prove essential to finding the true “first stars”. By coupling early chemical enrichment to evolving stellar spectra, the final model will provide detailed connections between early chemical evolution preserved in the Galactic halo and direct indicators at high redshift.

These three projects are all long-term goals of a final model only the beginning of steps of which are reported here, mainly related to Goal 1. This paper focuses on integrating Galactic chemical evolution into the hierarchical theory of galaxy formation. For now, I concentrate my efforts on laying out the model in detail and comparing its results for the Galaxy against detailed constraints from metal-poor stars and the requirements of reionization. As explained below, the initial focus is on deriving empirical constraints on the first-stars IMF, as a complement to purely theoretical approaches that are being pursued by many groups (Bromm et al. 2001; Abel et al. 2002; Omukai et al. 2005; Tan & McKee 2004).

Theory is conflicted on whether the first stars are exclusively very massive (I adopt here the formal definition  $M \geq 140 M_{\odot}$  for VMSs - see § 3.1.3). Abel, Bryan, & Norman (2002) first implemented rigorous H<sub>2</sub> cooling in a cosmological hydrodynamical simulation and found that the first star formed in their simulated volume was surrounded by several hundred solar masses of material that could have accreted, leading to the suggestion of stars with only  $M \gg 100 M_{\odot}$  in the first generation. Recent studies (Omukai & Palla 2002; Tan & McKee 2002), taking the Abel et al. result as a starting point for semi-analytic models of primordial star formation, indicate that primordial star formation may be complicated by feedback on the accreting material. Omukai & Palla (2002) identified a critical accretion rate ( $\dot{M} = 4 \times 10^{-3} M_{\odot} \text{ yr}^{-1}$ ) above which laminar accretion onto a spherically-symmetric protostar exceeds the Edington limit, when the star has  $M = 100 - 300 M_{\odot}$ . Models by Bromm & Loeb (2004) found a conservative upper limit of  $500 M_{\odot}$  by setting the time available to accretion to be the stellar lifetime ( $\sim 3 \times 10^6 \text{ yr}$ ) but ignoring feedback. Tan & McKee (2002) consider the effects of disk accretion geometry, rotation, and radiation feedback in limiting the mass of primordial stars. They find that these feedback mechanisms are likely to operate at  $M = 30 - 100 M_{\odot}$ , perhaps limiting the masses of metal-free stars to this range. However, they later found (Tan & McKee 2004) that none of the feedback mechanisms considered can halt the accretion before the star achieves  $\sim 30 M_{\odot}$ . Omukai et al. (2005) considered the effects of metals on the fragmentation of low-metallicity clouds, and suggest that a purely top-heavy IMF at  $Z = 0$  switches to a bimodal IMF at finite metallicities  $Z \lesssim 10^{-4}$  before settling to a more normal power-law function near  $Z \sim 10^{-2}$ . These important results indicate that the mass limits of the primordial IMF may be quite different from today. This intriguing yet unsettled guidance from state-of-the-art theory motivates this empirical approach to constraining the IMF of the first stars.

The IMF, as it is classically understood in the Galaxy today, is derived from counting stars in Galactic stellar

TABLE 1  
MODEL PARAMETERS AND THEIR FIDUCIAL VALUES

Parameter	Value	Description
Cosmology		
$\Omega_M$	0.27 <sup>a</sup>	Cosmic matter density
$\Omega_{\Lambda}$	0.73 <sup>a</sup>	Cosmological constant
$h$	0.71 <sup>a</sup>	Hubble parameter
$\Omega_b$	0.044 <sup>a</sup>	Baryon density
$\sigma_8$	0.84 <sup>a</sup>	Power spectrum normalization
$\delta_{c,0}$	1.686	Critical overdensity for collapse
Chemical Evolution		
$M_{\text{gal}}$	$5 \times 10^{11} M_{\odot}$	Total Galaxy mass
$\tau_{\text{disk}}$	$0.8 - 3 \times 10^8 \text{ yr}$	Disk formation timescale
$z_{\text{disk}}$	8 - 12	Halo cutoff redshift
$T_{\text{vir}}^{\text{min}}$	$10^3 - 10^4 \text{ K}$	Minimum virial temperature
$M_l$	$10^8 M_{\odot}$	Minimum mass resolution
$\epsilon_*$	$2 \times 10^{-10}$	Star formation parameter
$m_{\text{Fe}}$	$0.07 M_{\odot}$	Standard Type II iron yield
$Z_{\text{cr}}$	$10^{-4}$	Critical metallicity
$M_{\text{dil}}^0$	$10^6 M_{\odot}$	Interstellar dilution mass
$t_{\text{dil}}^0$	$10^7 \text{ yr}$	Interstellar mixing timescale
Intergalactic Medium		
$f_Z^{\text{esc}}$	0.05	Mass fraction of ejected metals
$M_{\text{IGM}}^{\text{dil}}$	$5.0 \times 10^8 M_{\odot}$	Final IGM metal dilution mass
$t_{\text{IGM}}^{\text{dil}}$	$5.0 \times 10^9 \text{ yr}$	IGM metal dilution timescale

<sup>a</sup>Spergel et al. (2003)

clusters. In some cases a single cluster is massive and young enough to sample the full IMF (see Figer 2005 for a state-of-the-art case). This technique is still feasible in regions of the local universe close enough to allow imaging of resolved stars, such as the Magellanic Clouds. Beyond this, the IMF is an abstraction that must be understood in a model-dependent fashion using indirect indicators such as galaxy colors and emission from H II regions. In these cases it may still be sensible to speak of the IMF as representing the spectrum of masses in a single, coeval cluster of stars. In the early universe, within small dark-matter halos that may have only  $10^5 - 10^7 M_{\odot}$  of gas and  $100 - 1000 M_{\odot}$  in stars, the IMF takes on a third distinct meaning. Here it is the parent probability distribution from which stellar masses are drawn stochastically based on their (indeterminate) initial conditions for star formation. As the initial conditions for star formation may vary from place to place, the parent probability distribution may also vary. However, theoretical efforts have identified the gas metallicity as the critical factor influencing the cooling, collapse, and fragmentation properties of low- or zero-metallicity gas (Bromm et al. 2002; Omukai et al. 2005), it is sensible to speak of a single probability distribution for zero-metallicity gas. Thus, the IMF is taken here to be the probability distribution of masses for stars formed from metal-free gas, wherever it exists.

The terminology in this paper maintains a distinction not usually seen in the theoretical literature. The designations “Population II” and “Population III” are historical observational definitions referring to detected and hypothesized populations residing the Galaxy today (Baade 1944). This definition is maintained here, and these

terms are used to denote only Galactic stars. The terms “metal-free” or “zero-metallicity” will refer to early stellar populations more generally by including those stars born early that were too short-lived to be around today. By this definition, a true Population III star is a (presumably low-mass) star with no metals that resides today in the Galactic halo. To date no Population III stars have been found.

I emphasize here that what follows is not a rigorous model for the formation of the Galaxy, intended to represent faithfully the actual mass assembly history, and in particular the dynamics, of the Galaxy. This is a model for Galactic chemical evolution following in the tradition of analytic chemical evolution models but motivated by and grounded in the hierarchical theory of galaxy formation. The model was created to take full advantage of present and future observational efforts to dissect the detailed assembly history of the Galaxy and to try to understand near-field signatures of early stars. Since the initial effort has met with some success, this model will, in the future, be extended to include dynamics and to cover a population of galaxies at arbitrary redshift, to connect it to high-redshift galaxy surveys (Goals 2 and 3). These extensions represent another leap in complexity, detail, and computing time, and so will be deferred to later papers. Until then, the reader must keep in mind the motivation and limitations of the model in assessing the conclusions.

The paper proceeds as follows. Section 2 describes the merger-tree structure formation model in detail. Section 3 describes the chemical evolution model including the assumptions and their motivations. Section 4 describes observational information that will be used to constrain the primordial IMF. The major results on the IMF are described in Section 5. Section 6 describes some additional results of the model that do not involve the IMF directly, including information about the epoch of the first stars. Section 7 discusses these results in the context of other theoretical results and present and future observational efforts to address these questions. Section 8 summarizes the key results and provides some additional comments on the future of studying the first stars.

## 2. A HIERARCHICAL MODEL FOR THE GROWTH OF STRUCTURE

The chemical evolution model consists of two major components. First, a model of hierarchical structure formation is used to decompose the present-day Galactic dark-matter halo into its constituent pieces, working backward in time. Once this process is complete the second component uses this mass assembly history to calculate histories for stellar populations and chemical enrichment, working forward in time. The structure formation component is described in this section, and the chemical enrichment calculations are described in § 3.

This section gives a brief introduction to the basic theory underlying the structure-formation model; more detail about the specific implementation is given in the Appendix. This model relies on a framework for following the hierarchical growth and mergers of dark matter halos over time that has been fully developed in the literature over the last three decades. The model primarily follows the method and notation of Lacey & Cole (1993; hereafter LC93), who developed the “extended

Press-Schechter” formalism for calculating halo merger probabilities and rates from the more *ad hoc* treatment of Press & Schechter (1974). For a thorough introduction and rigorous derivations of these relations, see LC93 or Liddle & Lyth (2000).

The extended Press-Schechter treatment of structure formation begins with a power spectrum of Fourier modes,  $P(k)$ , that describes the probability distribution of small ( $\delta \equiv \rho/\langle\rho\rangle \ll 1$ ) density fluctuations in the early universe. From early times these fluctuations grow linearly according to the linear growth function,  $\delta(x, t) = \delta(x, t_0)D(t)/D(t_0)$ , until  $\delta \sim 1$ , when the fluctuation is said to have entered the nonlinear regime, “turned around” and virialized. The overdensity of turnaround corresponds to a critical linear overdensity,  $\delta_c$ , that can be calculated by considering the evolution of an isolated spherical region (see Section 11.1 of Liddle & Lyth 2000). This linear density contrast is only weakly dependent on cosmological parameters; here  $\delta_c = 1.686$ . This critical density separates regions in the evolving linear field that have collapsed from those that have not.

The number density of collapsed halos is equivalent to number of density fluctuations that have achieved the critical linear density by the redshift of interest. The density field is first smoothed over some mass scale  $M$  to derive the variance of the density field as a function of smoothing mass,  $S(M)$ , using a spherical top-hat filter and performing the calculation in Fourier  $k$ -space:

$$S(M) \equiv \sigma^2(M) = \frac{1}{2\pi^2} \int_0^\infty P(k) \bar{W}^2(kR) k^2 dk, \quad (1)$$

where  $\bar{W}(kR)$  is the real-space top-hat window function. Further details of this calculation are given in the Appendix. From now on, I use the local (smoothed) variance as a function of mass,  $S(M)$ , to describe the density field. Generally,  $S(M)$  decreases as  $M$  increases and small wavelength density fluctuations are smoothed out. From here, the calculation will be considered in terms of a single mass element or test particle as the smoothing mass is varied, rather than the variations from place to place. At a given location, the variance  $S(M)$  executes a random walk as the smoothing mass is varied, occasionally crossing the critical barrier of  $\delta_c$ , where it is said to have collapsed. To avoid the so-called “cloud-in-cell” problem (LC93), the largest mass at which a given trajectory crosses this barrier is taken as the mass of the collapsed halo inside which the test particle resides. The number density of regions that lie above  $\delta_c$  is described by a diffusion equation with an absorbing boundary condition at  $\delta_c$ , leading to an expression for the number density of collapsed objects as a function of mass, the Press-Schechter formula:

$$ndM = \sqrt{\frac{2}{\pi}} \frac{\bar{\rho}}{M} \frac{\delta_c(z)}{\sigma^2(M)} \exp\left[-\frac{\delta_c^2(z)}{2\sigma^2(M)}\right] dM \quad (2)$$

where  $\bar{\rho}$  is the cosmic mean matter density. Further manipulation of this formula (LC93) gives the so-called “conditional mass function”, or the fraction of possible trajectories inside collapsed mass  $M_1$  at redshift  $z_1$ , that are also in halos with larger mass  $M_0$  at lower redshift  $z_0$ . This relation is given by LC93:

$$P(\Delta S, \Delta\omega)d\Delta S = \frac{1}{\sqrt{2\pi}} \frac{\Delta\omega}{(\Delta S)^{3/2}} \exp\left[-\frac{(\Delta\omega)^2}{2\Delta S}\right] d\Delta S \quad (3)$$

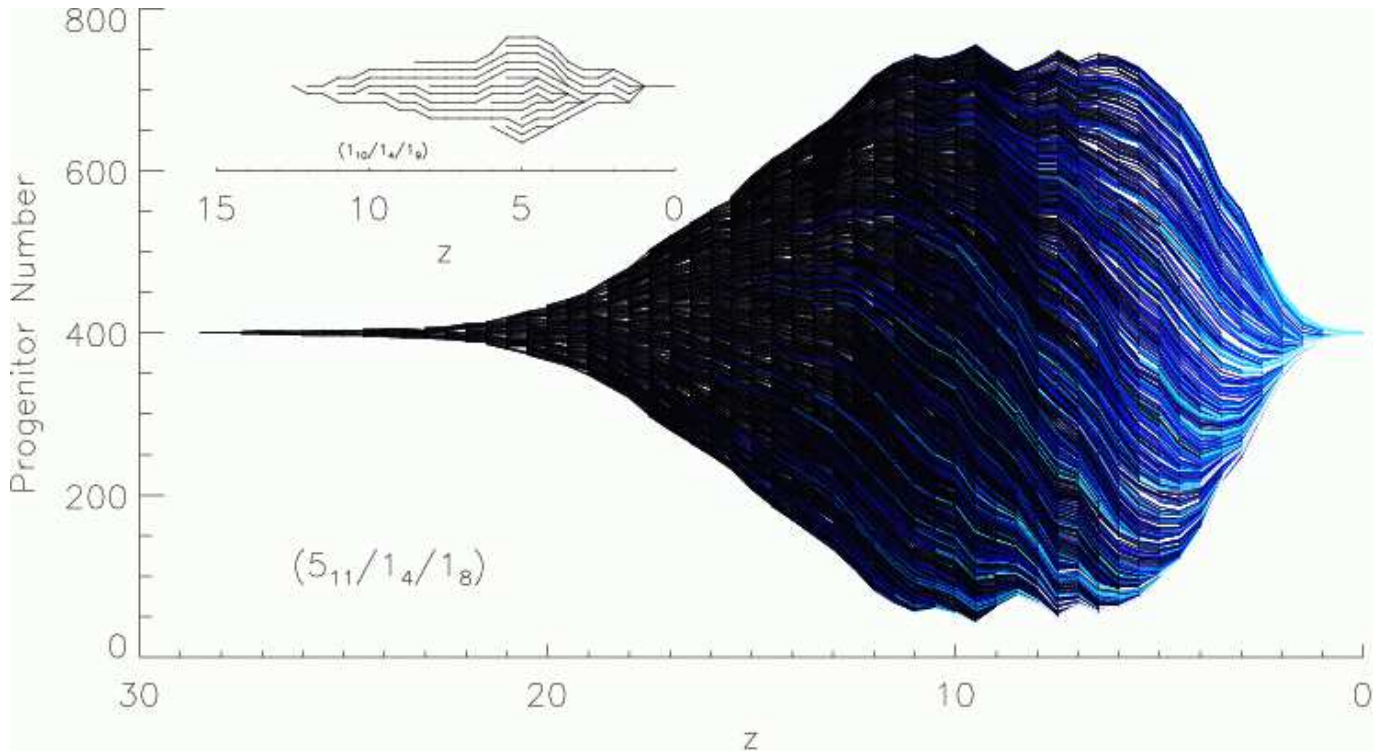


FIG. 1.— Examples of two halo merger trees. At  $z = 0$ , the larger final halo has  $M_h = 5 \times 10^{11} M_\odot$ . The tree was calculated with virial temperature resolution  $T_{vir}^{min} = 10^4$  K and mass resolution  $M_l = 10^8 M_\odot$ . The number of active progenitor halos peaks at  $z \sim 6 - 10$ , beyond which halos begin to drop below the finite virial temperature resolution, become “leaf” halos and so disappear from the tree. The color scale for the main tree expresses the halo mass increasing from black to light blue. The single halo at  $z = 23$  is the first-born progenitor of the Galaxy’s most massive immediate predecessor. The inset shows a smaller tree for illustration of typical branching behavior.

With a change of variables

$$x = \Delta\omega / \sqrt{\Delta S}, \quad (4)$$

this probability distribution assumes the form of a Gaussian with unit variance. Given a known redshift timestep ( $\Delta z \propto \Delta\omega$ ), this formula describes the probability distribution of “child” halos which compose the larger halo at lower redshift. This formula can be used to stochastically decompose a large low- $z$  halo progressively into smaller and smaller pieces in a halo merger tree.

The method for constructing trees follows the “N-fold merger with accretion” method devised by Somerville & Kollatt (1999). The construction of a merger tree begins with the choice of a final halo mass,  $M_h$ , at  $z = 0$ . For a model Milky Way, I choose  $M_h = 5 \times 10^{11} M_\odot$  (the final results will be shown to be insensitive to this choice). The merger tree is specified by  $M_h$  and the assumption of mass resolution and/or minimum virial temperature. At each redshift, the mass resolution is the smaller of  $M_l$  and  $M(T_{vir}^{min})$ . Beginning with the final halo at  $z = 0$ , I first derive a redshift interval over which to evolve the halo (the “timestep” equivalent to  $\Delta\omega$ , where  $\omega(z) = \delta_c(z)$ , see Appendix). This can be set to either a fixed value (usually  $\Delta z = 0.5$ ) or allowed to be redshift and/or mass dependent. This choice slightly affects the overall size of the tree.

Once the timestep is determined, the “parent” halo is disintegrated into its “child” halos according to the “N-fold with accretion” scheme developed by SK99. A random variant is drawn from Equation 3 after the change of variables and converted into child mass using equa-

tions Equations 1, 3, and 4. If this mass is greater than the smaller of  $M(T_{vir}^{min})$  and  $M_l$ , this halo is termed a “child” and its mass is subtracted from the reservoir. If this new halo mass falls below the mass cutoff, the random variant is drawn again. This procedure is repeated until the remaining mass of the parent is less than  $M_l$  or  $M(T_{vir}^{min})$ , at which point the parent halo has been divided into typically 2 - 5 progenitor halos and a parcel of “accreted” material. Halos that lie below  $M_l$  and/or  $T_{vir}^0$  at their redshift are termed “leaf” halos. The mass limit  $M_l$  is imposed to inhibit a large number of very low-mass progenitor halos at low redshift. A mass integral over all leaf halos and accreted mass equals the total mass of the final galaxy halo,  $M_h$ .

In the following discussion individual trees are labeled with their final halo mass  $M_h$ , minimum virial temperature  $T_{vir}^{min}$ , and absolute mass resolution  $M_l$  as  $(M_h, T_{vir}^{min}, M_l)$  using exponential notation such that  $1_8 = 1 \times 10^8$ . Thus a  $(5_{11}/1_3/1_8)$  tree models a dark matter halo with mass  $5 \times 10^{11} M_\odot$  at  $z = 0$ , decomposed into progenitor halos with minimum virial temperature  $10^3$  K or minimum mass  $M_l$ , whichever is lower at a given redshift.

To ensure that the method produces a distribution of halo masses that matches the original Press-Schechter function for the number density of halos, I create a “universe” of trees by drawing a large number (typically 10000) halos from the analytic EPS distribution at  $z = 0$ . Merger histories are then calculated for these halos and combined into a single distribution for comparison to the EPS function at any redshift (Equation 2). Good agree-

ment is found between the analytic halo mass spectrum and the numerical results. The numerical results calculated from the EPS formalism also agree well with the halo number-density and mass distributions presented by Mo & White (2002) when their fiducial cosmological parameters are adopted.

### 3. CHEMICAL EVOLUTION IN THE HIERARCHICAL CONTEXT

This section describes the chemical evolution model, including its relationship to the merger trees, the methods for calculating chemical evolution, and their assumptions. For halos in the merger tree, there are in essence only two processes that must be followed. These are halo evolution in isolation (§ 3.1) and halo mergers (§ 3.2). In addition, the transport of metals from virialized halos into new halos is followed in terms of a model IGM, which is described in § 3.3.

To calculate a chemical enrichment history for a merger tree, the driver starts with the earliest “child” halo ( $z = 23$  in Figure 1) and evolves it forward in time until a merger is reached. If all the child halos involved in that merger have had their evolution calculated, the merger occurs. If the child halos are not yet all calculated, the driver steps back to higher redshift until it reaches a leaf halo and uses that as a starting point for working forward until it reaches the potential merger where it stopped before. If all components of the potential merger are now calculated, the merger occurs. If not, the driver steps back, and so on. In this way the driver calculates the chemical enrichment history of all individual halos and merges them, such that the final  $z = 0$  halo is the last to be merged.

#### 3.1. Chemical Evolution of Isolated Halos

Between mergers, a halo in isolation evolves forward in time according to equations describing its stellar populations and gas mass and metallicity. Inside an isolated halo, these equations simply describe the rate at which gas is formed into stars, the IMF, the rates at which mass is returned to the ISM (in the form of ejected gas and metals), and the properties of mixing in the ISM. This evolution is managed by a driver which takes 10 - 50 uniform timesteps between the initial and final redshifts for the halo. I describe these methods here in detail.

##### 3.1.1. Star Formation Law

Gas residing in gravitationally bound dark matter halos is assumed to form stars at a fixed mass efficiency per year,  $\epsilon_*$ . The total mass in stars formed in a given time interval  $\Delta t$  is given by  $M_* = M_{gas} \times \epsilon_* \times \Delta t$ . The fiducial rate is fixed at  $\epsilon_* = 2.0 \times 10^{-10}$  for all halos to approximate the total gas mass ( $5 \times 10^9 M_\odot$ ) and stellar mass in the Milky Way for the final halo of a ( $5_{11}/1_3/1_8$ ) tree. Star formation is allowed to proceed, and is followed explicitly, only in those halos which have  $M \geq M(T_{vir}^{min})$  at their redshift. Child halos with less than this mass are considered to be diffuse “accreted” gas, which is placed into the halo in uniform parcels in each timestep during single halo evolution.

##### 3.1.2. Disk/Halo Mass Segregation

If all star formation down to  $z = 0$  is assumed to take place in the Galactic halo, and to deposit its stars

and ejected metals there, then the final model halo possesses many stars which properly belong in the Galactic disk and/or bulge. The semi-analytic galaxy-formation models on which this model is based (e.g., Somerville & Primack 1999) typically track the growth of a disk explicitly based on the angular momentum of accreted gas parcels, but this method would add too much complication and parametric freedom to this simple model. To reproduce the Galactic halo metallicity distribution function (MDF), it is necessary to introduce a simple prescription for when gas has settled into the disk. Two approaches to this problem are adopted here.

First, a single parameter,  $\tau_{disk}$ , can control the time after which a parcel of gas in the dark-matter halo has settled into the disk. Each parcel of gas in the tree, whether acquired by accretion or merger, has a time associated with it that measures the interval since it was virialized or accreted. When this time has reached  $\tau_{disk}$ , the parcel is moved into the disk and no longer forms halo stars. This parameter is the most sensitive control on the location of the peak for the halo metallicity distribution function (see § 4). For  $T_{vir}^{min} = 10^4$  and  $10^3$  K,  $\tau_{disk} = 0.8 - 3.0 \times 10^8$  yr gives the best fit to the peak. With this value, halos convert  $\tau_{disk} \times \epsilon_* \sim 2 - 6\%$  of their gas mass into stars before the gas enters the disk. This approach effectively imposes a fixed timescale *per halo* such that the cutoff occurs over a range of redshifts reflecting the varying birth times of halos. This approach is not limited to representing disk/halo segregation only - it can also stand in for the timescale after which gas no longer forms star because of SNe feedback or some other mechanism.

An alternative approach is to impose a fixed redshift after which all halo star formation ceases. This fixed redshift cutoff can also reproduce the basic peaked shape of the MDF (see § 4.1), for a cutoff fixed at  $z_{disk} = 8 - 12$  depending on  $T_{vir}^{min}$ . The disk timescale method produces a slightly better overall fit to the halo MDF than does  $z_{disk}$ . In some cases when both are included the overall fit is improved over the best fit if only  $\tau_{disk}$  is used, particularly at  $[\text{Fe}/\text{H}] < -1.0$  (where the data is uncertain - see RN91 and Section 4.1). Developing a rigorous method for mass segregation will require accurate treatment of the dynamics of the Galaxy formation process, which are completely absent from the present model but which will form a key component of a final model. Because the choice does not affect the primary constraints on the IMF discussed in § 4, I adopt  $\tau_{disk} = 0.8 - 3 \times 10^8$  yr in the fiducial model, and proceed.

##### 3.1.3. Stellar Initial Mass Function

The IMF is the most important ingredient for modeling early chemical enrichment. The IMF controls both the mass budget of metals released into the ISM and the number and mass distribution of low-mass stars that survive to  $z = 0$ . The IMF can take two forms: a power law with high and low mass limits, or a log-normal form with or without limits. The power law IMF has the form

$$\frac{dN}{dm} = m^{-\alpha} \quad (5)$$

For a Salpeter or “standard” IMF, the power-law slope is  $\alpha = 2.35$  (Salpeter 1955), and at least a lower mass limit must be assumed to keep the total number of stars finite.

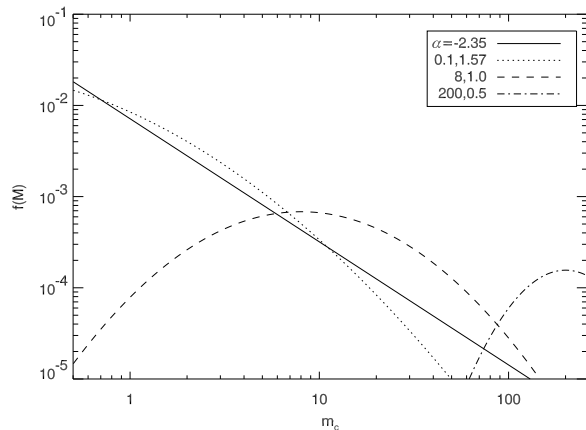


FIG. 2.— Examples of four different stellar initial mass functions, including a power-law IMF with  $\alpha = -2.35$  (solid), the Galactic Miller-Scalo IMF with  $m_c = 0.1$ ,  $\sigma = 1.57$  (dotted), a log-normal IMF with  $m_c = 8$ ,  $\sigma = 1.0$  (dashed), and a “strong VMS hypothesis” IMF with  $m_c = 200$ ,  $\sigma = 1.0$  (dot-dashed), all normalized to the same total mass.

This IMF has the advantage of a simple functional form and general agreement with observations of the local universe, and the drawback that it is too simple to describe a potentially wide range of probability distributions that may obtain in the early universe. The log-normal IMF (Larson 1973) takes the form:

$$\ln\left(\frac{dN}{d\ln m}\right) = A - \frac{1}{2\sigma^2} \left[ \ln\left(\frac{m}{m_c}\right) \right]^2 \quad (6)$$

where  $\sigma$  is the width of the distribution,  $m_c$  is the characteristic mass, and  $A$  is an arbitrary normalization. This IMF has the advantage of more flexible behavior with only one additional parameter. This study uses lower and upper mass limits of 0.5 and  $260 M_\odot$ . The mean mass for a given pair of log-normal IMF parameters is slightly higher than the characteristic mass  $m_c$  because of the adopted lower mass limit of  $0.5 M_\odot$ .

I adopt here the “VMS hypothesis”, as introduced and defined by TVS04. Under this definition, “very massive stars” (VMSs) are those with  $M \geq 140 M_\odot$ , the smallest mass at which the pair instability can completely disrupt the star and leave an unusual nucleosynthetic signature (Heger & Woosley 2002, hereafter HW02). Stars with 8 -  $140 M_\odot$  are “massive stars” with yield patterns characterized by Type II supernovae. This upper limit for massive stars is slightly higher than the  $100 M_\odot$  conventionally used in simple stellar population studies (Starburst 99; Leitherer et al. 1999) for the Galaxy and the nearby universe, but there are suggestions that some such stars exist today. Figer (2005) has recently established a firm upper limit of  $150 M_\odot$  for the Galactic Arches cluster, which contains at least one star of  $130 M_\odot$ . Thus  $140 M_\odot$  serves as a natural dividing line on both theoretical and observational grounds.

There are two different versions of the VMS hypothesis that are distinguished by their different nucleosynthetic patterns. The “strong” VMS hypothesis holds that metal-free stars formed only with  $M \gtrsim 140 M_\odot$ , or more technically, that VMS are the only stars in the IMF that leave a nucleosynthetic signature. In the “weak”

VMS hypothesis, the 8 -  $40 M_\odot$  progenitors of Type II supernovae form in addition to VMS. In TVS04, this definition was rigidly constructed and the two versions were expressed in terms of an IMF that was truncated at either  $140 M_\odot$  (“strong”) or  $10 M_\odot$  (“weak”). Here the definition is loosened slightly by dropping the strict truncations in favor of a log-normal IMF. Examples of these IMF shapes appear in Figure 2. The distinction now depends on which mass range, and therefore which type of supernova, dominates the production of metals, with “dominance” nominally taken to mean one-half the budget of iron. These considerations are used below to constrain the early IMF in detail.

### 3.1.4. Critical Metallicity for Normal Star Formation

Most of the unique behavior associated with primordial star formation follows from the unique circumstances of cooling by zero-metallicity gas. At  $T \lesssim 10^4$  K in the local interstellar medium, cooling by H and He is negligible and metal-line cooling is dominated by [C II], [O I], and [Si II] fine-structure lines. Because metal-free gas is restricted to inefficient cooling by  $H_2$  at  $T \lesssim 10^4$  K, cooling rates are reduced, and the balance between pressure support and gravitational collapse is shifted to higher temperatures. Primordial protostellar objects, being unable to cool or fragment, should therefore be more massive to overcome their elevated gas pressure. At critical metallicity  $Z \gtrsim 10^{-5.5} - 10^{-3.5} Z_\odot$ , protostellar clouds are able to cool and fragment more efficiently, leading to a “normal” IMF (Schneider et al. 2002; Bromm & Loeb 2003). This metallicity may not be fairly represented by a single value, if the yields of early SNe are highly variable and the first metal-enriched star forming regions incorporate only a few SNe in stochastic fashion (Santoro & Shull 2005). For simplicity this model assumes that  $Z_{crit}$  is expressed as a single [Fe/H] as a parameter of the model. There is a capacity to switch the IMF at a single  $Z_{crit}$ , which happens at different times in different halos and so spans a range of redshifts.

### 3.1.5. Stellar models and supernova metal yields

Stellar lifetimes are specified by an analytic fit to the  $Z = 0$  H-burning main sequence lifetimes specified in Table 2 of Tumlinson, Shull, & Venkatesan (2003). Type Ia thermonuclear SNe are formally included with  $m_{Fe} = 0.5 M_\odot$  but generally enter too late to affect subsequent star formation in the halo, considering the timescale for disk/halo segregation. All massive stars with  $M = 8 - 40 M_\odot$  experience core-collapse SN at the end of their lifetimes (HW02) and release  $0.07 M_\odot$  of iron into the parent halo. Detailed yields for pair-instability supernovae (PISNe) are taken from HW02.

### 3.1.6. Metal dispersal and mixing

Metal mixing in the interstellar medium is another important factor in chemical evolution. The first key assumption about metal dispersal is that the “boxes” that represent dark matter halos are closed and metals do not escape (except for the small fraction represented by  $f_{esc}^Z$  that escape to the IGM). This leaves two avenues by which halos acquire metals. First, metals produced by local SNe are released into the gas and enrich subsequent generations. Second, when new halos virialize

from the IGM, they bring along gas that may be metal-enriched (see § 3.3). This key assumption of closed boxes has many effects on chemical evolution and may in fact be violated in some cases (see discussion of minihalos in Section 5.5).

Rather than attempt to follow the complicated details of supernova remnant evolution in a clumpy medium (e.g., Oey 2000), this model accounts for the cumulative effects of SN enrichment in terms of mass only, and in a stochastic fashion. There are two basic principles behind the treatment of mixing: (1) that the mass into which the ejecta of a single supernova are mixed grows steadily over time before asymptotically approaching a fixed maximum dilution mass, and (2) that new star formation randomly samples metals from the parcels of mass enriched by previous generations, allowing for maximum statistical fluctuations in the metallicity distribution of new stars. Principle 1 provides a simple mechanism for tracking metal enrichment that elides many of the complicated details of interstellar physics. Of course, this approach may omit other useful information, but it is necessary to make this model tractable and executable in short times. Principle 2 provides maximum flexibility, in that individual SN can be treated as completely uncorrelated. Various degrees of correlation can be introduced to make the model more deterministic and perhaps more representative of clustered or triggered star formation, while a model designed to follow clustered or triggered star formation explicitly could not be tuned for more stochastic behavior.

For each massive or very massive star the time of its SN,  $t_{SN}$ , is stored. After this time is reached, the ejected metals are assumed to have been released into the interstellar medium of the parent halo, and diluted into a dilution mass at a later time  $t$ :

$$M_{dil}(t) = M_{dil}^0(1 - e^{(t_{SN}-t)/t_{dil}^0}), \quad (7)$$

This “dilution mass” is then divided by the halo gas mass to derive the mass fraction of the total halo mass into which the products of each supernova have been evenly mixed. Where the dilution mass exceeds the total gas mass of the parent halo, the mass fraction is truncated at unity (embodying the assumption of closed boxes). Then a vector of random variants is drawn with as many elements as there are SNe. Where these random variants lie within the mass fraction enriched by an SN, that SN contributes to the total metal budget for the stars formed in that timestep. For the fiducial models,  $M_{dil}^0 = 10^6 M_\odot$  and  $t_{dil}^0 = 10^7$  yr. These parameters have been set to express the values expected for the growth of supernova remnants in the Galactic ISM during the radiative phase (Spitzer 1978). This generally leads to a monotonic enrichment for massive halos but can yield highly stochastic results in the first small halos. In the limit of small  $t_{dil}^0$  or large  $M_{dil}^0$ , the mixing approaches an instantaneous limit that is useful for exploring some limiting cases.

### 3.2. Merging multiple halos

Halo mergers are pairwise sums over all the progenitor halos and so simply inherit all their progenitors’ stars and gas. Mergers affect the evolution only indirectly by providing a larger dilution mass for metals previously released into the gas reservoirs of the merger partners.

### 3.3. The Intergalactic Medium

After halo self-enrichment by local star formation, halo-halo cross-enrichment by metal transport across the IGM is the second possible mechanism by which halos acquire metals. There are two forms of halo cross-enrichment - the accretion of metal-enriched IGM gas by an already virialized halo, and the formation of a halo from gas that has already been enriched by previous generations of star formation. These avenues to metal enrichment involve the complicated processes of metal ejection from virialized halos, their dispersal and mixing into the IGM, and their incorporation into nearby existing or future halos, for which there is little observational information at high redshift and no self-consistent theory.

Previous studies of chemical evolution and IGM metal enrichment vary in their approach to the problem, with their conceptions of the IGM being the major discriminant. Oey (2000) treats this problem in the context of an inhomogeneous chemical enrichment model - metals are transferred across space to nearby star formation regions, but since these are not termed “halos” the “IGM” is not explicitly included. The other approach is represented by Scannapieco et al. (2003) and Aguirre et al. (2003), who explicitly consider halo-halo cross-enrichment in the context of a hierarchical semi-analytic model (the former) or post-processed hydrodynamical simulations (the latter). If the hierarchical model of galaxy formation is correct, then the Oey approach, which tracks metal expulsion, transport, and mixing into nearby star formation regions, is sensible with only semantic changes to relabel star forming regions into halos and so on. With this adjustment the two approaches can be considered on roughly equal footing with respect to observational constraints, and considered in this light they have advantages and weaknesses. Their parametric nature allows them to be suitably tuned to match the available data, but the relatively large number of parameters (10, in the case of the Aguirre et al. galactic wind model) used to capture the various physical processes limits their utility to a model like this one. However, the paucity of observational constraints on the distributions of metals in the IGM at  $z > 5$  means that virtually any model will have these limitations. It is therefore advisable to make the model only as complicated as is needed to accomplish its role in the larger model under development.

This “minimal model” tracks the distribution of gas metallicities in the IGM in terms of a cumulative filling factor as a function of redshift. For this purpose I use a very simple parametric model of the IGM, tuned to match the best available observational constraints at  $z = 3$ . The model IGM is calculated independently of the merger trees and so serves as a sort of “background” in which the main model evolves. The model follows the mass budget of metals expelled into the IGM by virialized halos, whose space density and mass function are described by the extended Press-Schechter formalism laid out in Section 2, using the same star formation law and other related assumptions used for single halo evolution to calculate an individual halo’s star formation history. Metals produced during this star formation history are explicitly followed and a mass fraction  $f_{esc}^Z$  of these are assumed to escape by one of the viable ejection mecha-



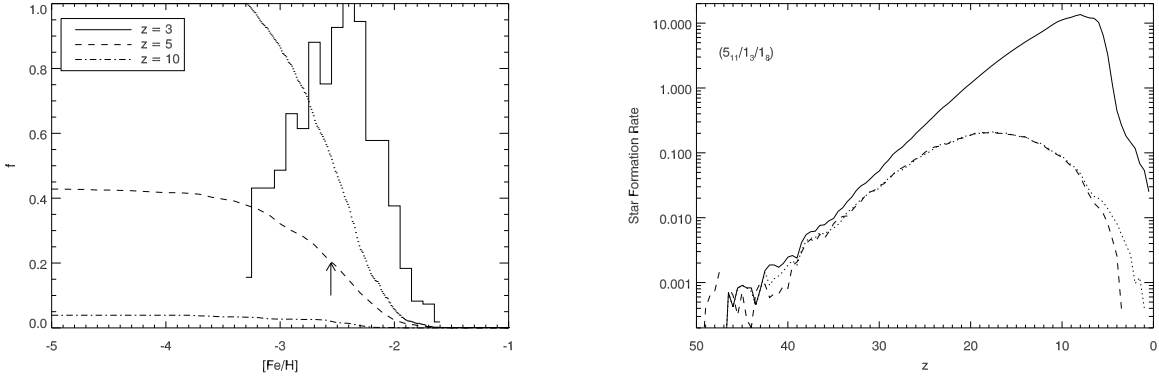


FIG. 3.— Left panel: The cumulative distributions of IGM metallicity  $f(Z)$  from which new halos are drawn, shown at  $z = 3$  (dotted),  $z = 5$  (dashed), and  $z = 10$  (dot-dashed) for the fiducial parameters  $(f_{esc}^Z, M_{dil}^0, t_{dil}) = (0.05, 58, 59)$ . This model has been tuned to approximate the  $\delta \sim 10 - 100$  curves in Figure 14 of Schaye et al. (2003), corresponding to overdensities similar to those of non-linear fluctuations near virialization. Right panel: The halo star formation rate for stars of all metallicities (solid) and  $Z = 0$  only with the IGM (dashed) and without the IGM (dotted). The overall SFR is the same with and without the IGM. The IGM modestly inhibits the formation of zero-metallicity stars below  $z \simeq 10$ , after the peak caused by disk/halo separation.

nisms, most likely supernova-driven winds (Madau, Ferrara, & Rees 2001) or halo-halo interactions (Gnedin 1998). Each “parcel” of metals driven from a single halo is then mixed into a time-dependent dilution mass, given by the same expression as for the ISM (see Eq. 7) but using the IGM parameters listed in Table 1. The single parameter set  $(f_{esc}^Z, M_{dil}^{IGM}, t_{dil}^{IGM})$  describes the model uniformly for all halos - the only mass or redshift dependence to these quantities is imparted indirectly by the star formation histories. These are calculated stochastically for evolving halos in a representative volume of the universe from  $z = 70$  to  $z = 0$ . By a single redshift, a given halo will have ejected a number of metal enriched parcels according to its individual star formation history. Each of these will be mixed into a dilution mass appropriate to its time since ejection.

At each redshift, the existing metal-enriched regions from all galaxies is randomly sampled to derive a probability distribution of mass filling factors for metal-enriched gas as a function of metallicity. During the random sampling, all the metal enriched regions from a single halo are assumed to be perfectly correlated or “nested”. That is, the smallest enriched mass associated with a given halo (the most recent one to be ejected) are assumed to reside entirely within the metal-enriched regions from previous timesteps. If the random sampling picks one of these less massive regions, the metallicity for that sample is given by the sum of all metals from that *and previous* metal-enriched parcels with larger dilution masses. This key assumption has two justifications. First, it seems reasonable to assume that since galaxies are the sources of metal enrichment, their successive generations of metal enrichment are highly correlated, or overlapping, in space and/or mass. Second, if each successive generation of metal ejection from a single halo is treated independently, the overall IGM is enriched too quickly to agree with observations at  $z = 3$ .

The above procedure is used to calculate a cumulative distribution of metals, integrated over all halos in a representative volume of the IGM, in terms of a filling factor  $f(Z, z)$ . This is done for a fixed grid of redshifts

from  $z = 70$  to  $z = 0$  with  $\Delta z = 0.5$ . This distribution of filling factors over redshift and metallicity is used sampled stochastically to find the metallicity of new halos, or accreted mass, in the halo merger tree chemical evolution model. The fiducial parameters have been tuned to  $f_{esc}^Z = 0.05$ ,  $M_{dil}^0 = 5 \times 10^8$  yr, and  $t_{dil} = 5 \times 10^9$  yr to match the  $\delta \sim 10 - 100$  filling factor curves at  $z = 3$  from the observational study of intergalactic C IV by Schaye et al. (2003), assuming  $[C/Fe] = 0.0$ . These curves correspond roughly to the non-linear overdensity of fluctuations near virialization, and so correspond to gas near galaxies that is likely to be metal-enriched and eligible for later collapse into new halos. The effect of the IGM is modest for the highest redshifts, as seen in Figure 3, which shows the redshift distribution of metal-free star formation with and without the IGM. The IGM has its largest effect at  $z \lesssim 5$ , and its effects are minimized when disk/halo segregation is included. However, the IGM may become important later in the model and so it is always used.

After this description of the major ingredients of the chemical evolution model, it is time to introduce the observational constraints that will be used to derive specific conclusions about the chemical evolution of the galaxy and the first generations of stars.

#### 4. OBSERVATIONAL CONSTRAINTS ON EARLY CHEMICAL EVOLUTION

The model is constructed to be tested against many different types of observations, following the theme of relating all observable quantities to one another. This section describes the various classes of observations, their power and limitations, and their connection to the model. Table 2 summarizes the basic information and the constraints they provide on the primordial IMF.

##### 4.1. Metal-poor Galactic Halo Stars

These old stars represent the first major observational window into early stellar populations, as they are perhaps more direct tracers of the early IMF than are the distant, indirect, and uncertain signatures of reionization. Beers & Christlieb (2005) give a thorough review

of the properties of Galactic metal-poor stars. I restate here only the most important features that bear on the present analysis. These are (1) the shape of the Galactic halo MDF, (2) the specific Fe-peak element ratios (especially Zn), (3) the widespread presence of  $r$ -process elements, and (4) elevated [C,N,O/Fe] ratios. This paper adopts the terminology of Beers & Christlieb (2005), who label stars according to their [Fe/H] like so: [Fe/H] < -2.0 is “very metal poor” (VMP), [Fe/H] < -3.0 is “extremely metal-poor” (EMP), [Fe/H] < -4.0 is “ultra-metal poor” (UMP), [Fe/H] < -5.0 is “hyper-metal poor” (HMP), and, should any exist, [Fe/H] < -6.0 are “mega metal-poor” (MMP).

*Galactic halo MDF:* The first key observable derived from the metal-poor halo stars is the overall metallicity distribution function. The observed MDF (Ryan & Norris 1991, hereafter RN91) has three important properties - a rise from [Fe/H]  $\sim$  -4 to a peak at [Fe/H]  $\approx$  -1.8, and a decline at higher metallicity. RN91 state that because disk stars are difficult to separate conclusively from the halo sample, stars above [Fe/H] = -1.0 are unreliable. Despite this limitation, the RN91 MDF is still the most complete in the literature, but will soon be superseded by larger samples from SDSS and other surveys (T. Beers 2005, private communication). This study focuses on the [Fe/H] < -2 portion of the MDF and on constraints that are insensitive to the behavior of the MDF above the peak at [Fe/H]  $\sim$  -1.8.

In addition to the shape of the MDF, the observed limit on the number of true Population III stars in the Galactic halo is a key constraint on the IMF of the first stars. The important quantity is  $F_0$ , the number of truly metal-free stars known in the Galactic halo divided by the total number at [Fe/H]  $\leq$  -2.5. This quantity is similar to the  $F_{III}$  used by Oey (2002) to examine the implications of Population III non-detections for Galactic chemical evolution, but with an important difference. Oey defined  $F_{III}$  to be the fraction of truly metal-free stars (1, to set a limit) divided by the total number in the halo sample, which was derived from the Beers et al. (1992) survey of 373 halo stars with [Fe/H] < -2.5 corrected for the Carney et al. (1996) result that 16% of all halo stars have [Fe/H] < -2.5. Thus  $F_{III} < 4 \times 10^{-4}$ .  $F_0$  is a slightly different metric that expresses the fraction of truly metal-free stars relative to the total *below* [Fe/H] < -2.5 in the halo sample. This difference in normalization has a two-fold justification. First,  $F_{III}$  may be contaminated by the ambiguous stars at [Fe/H] > -1.0, some of which may belong in the thick disk. Second, the details of the model MDF above the peak at [Fe/H]  $\sim$  -2 are sensitive to the method and assumptions by which gas is segregated from the halo into the disk ( $\tau_{disk}$ ), or by a halo cutoff redshift ( $z_{disk}$ ). Because both observations and theory are uncertain above the peak of the MDF, it makes sense to define a more robust metric. The limit on  $F_0$  is then given by the inverse of the total number of halo stars with [Fe/H] < -2.5. The 373 stars reported by Beers et al. (1992), and the 146 Hamburg-ESO survey stars reported by Barklem et al. (2005) yield  $F_0 \leq 0.0019$ . This limit is used below to provide detailed constraints on the IMF at  $Z < Z_{crit}$ .

*Iron-peak elements (Cr - Zn):* These elements are produced in explosive events and so trace nucleosynthesis by massive stars. Large samples presented by McWilliam et

al. (1995) and Carretta et al. (2002) found that the Fe-peak ratios to Fe, i.e. [Zn/Fe], qualitatively change their behavior at [Fe/H]  $\simeq$  -3, but the more recent high resolution studies by Cayrel et al. (2004) and Cohen et al. (2004) have found lower scatter and a smooth rather than abrupt change in the abundance ratios at [Fe/H]  $\simeq$  -2 to -4. In any case, the overall abundance pattern is consistent across the different studies. Theoretical yields of iron peak elements from metal-free stars have been calculated by a number of groups (e.g., HW02 for VMSs; Umeda & Nomoto 2005 for core-collapse SNe). These yields are sensitive to the energy, rotation, mass cut, and asymmetry of the supernova and to the pre-SN stellar properties. The models can be tuned to match individual observed abundance patterns by varying these assumptions. Because of these sensitivities and the remaining disagreement between different codes and investigators, and the intrinsic difficulty of calculating yields *a priori*, this study does not rely on detailed comparisons between theoretical yields of core-collapse SNe and observations of metal-poor stars to constrain the IMF, except in one case which makes use of a unique and widely agreed circumstance for zinc (see § 5.3). Instead this study has the ultimate goal of extracting intrinsic yields directly from the data, guided by models of chemical evolution.

*r-Process elements (A > 60):* These elements are produced by rapid neutron captures in hot, dense, neutron-rich explosive events. Although the exact physical sites are still uncertain, the proposed mechanisms are all associated with massive stars in the range  $M = 8 - 40 M_{\odot}$  and may be isolated to  $8 - 12 M_{\odot}$  (Truran et al. 2002). The existing samples of metal-poor stars show  $r$ -process elements down to [Fe/H]  $\sim$  -3.5 (McWilliam et al. 1995; Burris et al. 2000; Barklem et al. 2005). The mean [r/Fe] is similar to the solar value at all [Fe/H], but with scatter steadily increasing to 2 dex at [Fe/H]  $\sim$  -3. The relative abundances (i.e., [Eu/Ba]) are similar enough to the solar ratios to suggest that the details of the  $r$ -process are unchanged over more than 3 decades of metallicity (Truran et al. 2002). TVS04 argued that the presence of  $r$ -process elements in the EMPs effectively rules out the strong VMS hypothesis because PISNe do not experience the conditions in which these elements are created. For this reason the strong VMS hypothesis is not treated in detail here.

*Primary elements (C, N, O):* Some UMP stars are highly enriched in carbon relative to iron. This group includes the two most iron-poor stars known, HE 0107-4342 (Christlieb et al. 2003) and HE 1327-2326 (Frebel et al. 2005), both of which have [C/Fe] > 2.0. These stars appear to be *iron-poor*, rather than *metal-poor*, and therefore less chemically primitive than [Fe/H] indicates. Carbon is likely the dominant coolant that determines the IMF in the early ISM (Bromm & Loeb 2003) and the nuclear burning catalyst that determines by its absence the unusual evolution and radiation of the first stars (TSV03). These factors favor C instead of Fe as the “reference element” for finding chemically primitive stars in the local universe. No attempt is made here to explain these unusual stars on their own, and they are not included in the MDF sample.

The features of the metal-poor stars discussed here provide many interesting constraints on the history of chemical evolution in the Galaxy and on the first stars. Some

of these constraints, such as those provided by  $F_0$  and the large r-process enhancements down to  $[\text{Fe}/\text{H}] \sim -3$ , are quite robust and are not sensitive to the model. By contrast, making detailed use of the Fe-peak ratios requires some detailed knowledge of intrinsic SNe yields. These constraints are less robust because they are sensitive to the details of the specific theoretical model from which they are derived. This model is directed at extracting SNe yields directly from the data, so it is best to avoid constructing a model which depends on pure theoretical yields for its connection to the data. Nevertheless there are some reasonable constraints that can be drawn from the specific metal-abundance patterns and theoretical yields, where these are thought to be sound. These results are presented below with appropriate caveats.

#### 4.2. Reionization

The reionization of the IGM at high redshift is a key indicator of cosmic star formation activity at  $z \gtrsim 6$ . There are two major data that guide models of reionization. First, the Gunn-Peterson effect has been detected in the spectra of  $z \gtrsim 6$  quasars, indicating that the epoch of reionization ended near  $z = 6$ . Second, the unexpectedly high electron-scattering optical depth to the cosmic microwave background found by *WMAP*,  $\tau_{es} = 0.17^{+0.08}_{-0.07}$ , suggests that reionization began quite early and may have had a complicated history. Most of the ionizing photon budget that reionizes the IGM is thought to be produced by massive stars, as the number density of bright QSOs at that time is probably not sufficient (Loeb & Barkana 2001). However, there is not widespread agreement about the details of when reionization began, how it proceeded, and how galaxies of different mass and metallicity contributed to the process. A number of recent studies have approached this problem with semi-analytic models of the growth of structure and the evolution of cosmological H II regions into the IGM with varying assumptions and different results (Haiman & Holder 2003; Cen 2003; Venkatesan, Tumlinson, & Shull 2003). All these models have two common conclusions: (1) that the overall efficiency of converting baryonic mass to ionizing photons must be higher than for a metal-free stellar population with a Salpeter IMF between 1 - 100  $M_\odot$ , and (2) that “minihalos” with  $T_{vir} \leq 10^4$  K, where most of the high-redshift baryons reside, must participate in reionization if the *WMAP*  $\tau_{es}$  is to be reproduced.

TVS04 studied the ionizing properties of different IMFs and argued that a standard IMF deficient in low- and intermediate-mass stars could be just as efficient as VMSs at reionizing the IGM. In a stellar population synthesis, the quantity most relevant to reionization is the total number of ionizing photons produced per baryon locked into stars. If integrated over the lifetimes of the stars, this number is called  $\gamma_0$ . According to Figure 2 of TVS04, this quantity peaks at  $\simeq 120 M_\odot$  for metal-free stars, and then declines at higher mass. For a Salpeter IMF from 0.5 - 140  $M_\odot$ ,  $\gamma_0 = 17000$ . This value is generally not sufficient to reproduce the  $\tau_{es} \geq 0.10$ , while TVS04 showed that a similar IMF truncated at  $M = 10 M_\odot$  yields  $\gamma_0 = 65000$  and can produce  $\tau_{es} = 0.11 - 0.13$  without extreme assumptions for star formation efficiency ( $f_*$ ) or the Lyman continuum escape fraction ( $f_{esc}$ ). The TVS04 underlying struc-

ture formation model is based on the same extended Press-Schechter formalism, and the overall assumptions about star formation efficiency are comparable. Thus for this study I simply interpolate between the different IMF cases presented in TVS04 and conservatively require that  $\tau_{es}$  achieve the minimum value consistent with the *WMAP* data at  $1\sigma$  confidence,  $\tau_{es} \geq 0.10$ . In the TVS04 models, this requires  $\gamma_0 \geq 34000$ . These results appear in § 5. A full treatment of the detailed interrelationships between chemical evolution and reionization is enabled by this framework and certainly warranted, but it is too involved to take place here.

### 5. CONSTRAINTS ON THE PRIMORDIAL IMF

The IMF is, perhaps, the most fundamental feature of a stellar population, and therefore it is the most important fact of chemical evolution. For the same reasons, the IMF has many observable consequences. Some of these are used here to constrain the IMF of the first stars. This discussion starts with the most robust observational results and the strongest connections between data and theory, and then proceeds to the more model-dependent connections and looser observational constraints. The basic constraints and their results are summarized in Table 2.

#### 5.1. Constraints on the IMF from the Galactic Halo MDF and Population III Stars

The Galactic halo MDF is the first key result of the model. Good fits to the peak of the MDF are obtained for  $\tau_{disk} = 8 \times 10^7 - 3 \times 10^8$  yr for  $T_{vir} = 10^3$  and  $10^4$  K, respectively, when no halo cutoff redshift  $z_{disk}$  is assumed. The MDF can be fitted with reasonable parameters with or without minihalos (see Section 5.5), leaving the minimum virial temperature uncertain. These fits work well below  $[\text{Fe}/\text{H}] < -1.0$ , above which the MDF is declared unreliable by RN91. The fit in this region can be improved by the introduction of  $z_{disk} = 8 - 12$  (see § 3.1.2) with no effect on  $F_0$ . The best-fit MDFs for (5<sub>11</sub>/1<sub>3</sub>/1<sub>4</sub>) and (5<sub>11</sub>/1<sub>4</sub>/1<sub>8</sub>) trees are shown in Figure 4. This basic agreement between the observed and model MDFs provided encouraging evidence that the overall the model is an accurate description of early Galactic chemical evolution.

Another important quantity derived from the MDF is  $F_0$ , the number fraction of true “Population III” stars seen in the Galactic halo. The first key result from  $F_0$  is that the qualitative change in the IMF expressed by  $Z_{crit}$  must exist. If no  $Z_{crit}$  is employed, the IMF is the same at all metallicities and  $F_0 \gtrsim 0.1$  for IMFs ranging over (1.0, 1.0) to (100, 2.5). For a Miller-Scalo IMF (0.1, 1.57) at all metallicities, the model gives  $F_0 = 0.48$  for standard ISM mixing parameters and 0.25 in the instantaneous mixing limit. A Salpeter IMF with minimum mass 0.5  $M_\odot$  gives  $F_0 = 0.45$  for standard mixing and 0.23 for instantaneous mixing. These values are clearly excluded by the data, and so there must be an evolution in the IMF that inhibits the formation of low-mass stars below some finite metallicity. The observations require a  $Z_{crit}$ , although its specific value cannot be constrained below the most metal-poor star in the sample (see below).

For the fiducial  $Z_{crit} = -4.0$ ,  $F_0$  varies dramatically across the range of IMF parameters and so provides a critical constraint on the IMF at the low-mass end. Fig-

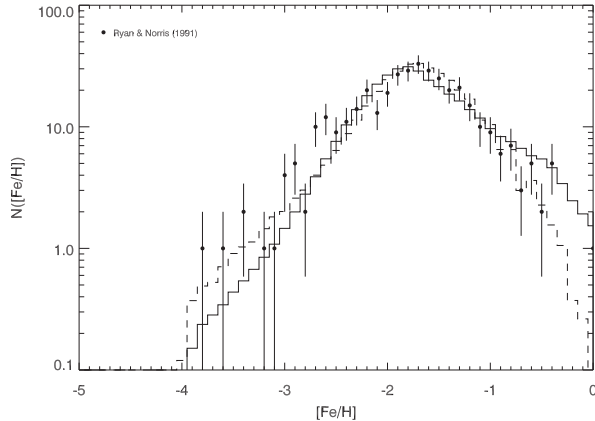


FIG. 4.— Comparison of theoretical MDFs for the fiducial ( $5_{11}/1_3/1_8$ ) tree (solid) and the fiducial ( $5_{11}/1_4/1_8$ ) tree (dashed) to the RN91 MDF for a log-normal IMF (10, 1.0) below  $Z_{crit} = -4.0$ . Both the model and observed MDFs are uncertain above  $[\text{Fe}/\text{H}] \sim -1.0$ .

ure 5 shows the variations of  $F_0$  with total halo mass,  $M_h$ , and minimum virial temperature  $T_{vir}^{min}$  (see Section 5.5 regarding the importance of minihalos with  $T_{vir} \leq 10^4$  K), with the curve for  $F_0$  plotted on the same scale but divided by ten. Variations in  $F_0$  with IMF overwhelm uncertainty in the other parameters and make  $F_0$  a robust constraint on the IMF that should only improve with new samples of metal-poor stars (until a truly metal-free star is directly detected). Of all the constraints used here, this one is least subject to astrophysical uncertainties and effectively has no model dependence. These results are displayed in panel A of Figure 6 over a large range of IMF parameters and the fiducial ( $5_{11}/1_3/1_8$ ) tree. The line marking  $F_0 = 0.0019$  passes through (4.0, 0.6) to (8, 1.5) before passing out the top of the frame. Thus  $F_0$  provides a strong requirement that the initial IMF is top-heavy, with  $m_c \gtrsim 6 M_\odot$  and mean mass of  $\langle M \rangle \gtrsim 8 M_\odot$ . In this parameter space, the Miller-Scalo Galactic IMF has  $m_c = 0.1$ ,  $\sigma = 1.57$ , and  $\langle M \rangle \approx 0.64 M_\odot$ . Thus our strongest constraint on the IMF,  $F_0$ , implies an IMF with mean mass at least 10 times that found in the present day.

The MDF may also contain evidence of the expected “critical metallicity” at which interstellar cooling becomes dominated by metal lines. For a single  $Z_{crit}$ , this signature would be expected to take the form of a noticeable break in the MDF at a single  $[\text{Fe}/\text{H}]$ . Inspection of Figure 4 shows that such a break is not apparent in the RN91 MDF, which has only 10 stars at  $[\text{Fe}/\text{H}] \leq -3$ . However, there could still be an indication of a statistically significant deficit of low- $[\text{Fe}/\text{H}]$  stars relative to expectations from the model. This is done by constructing the *cumulative* metallicity distribution, integrating up from zero metallicity to  $[\text{Fe}/\text{H}] = -2$ . For this test, the model MDF is normalized to have the same total number of stars at  $[\text{Fe}/\text{H}] \leq -2$  as the RN91 MDF (125 stars).

The results of this test appear in Figure 7, which shows cumulative MDFs for RN91 and the fiducial ( $5_{11}/1_3/1_8$ ) tree and four different values of  $Z_{crit}$ . A model with  $Z_{crit} = 10^{-5.0}$  overproduces EMP stars, while  $Z_{crit} =$

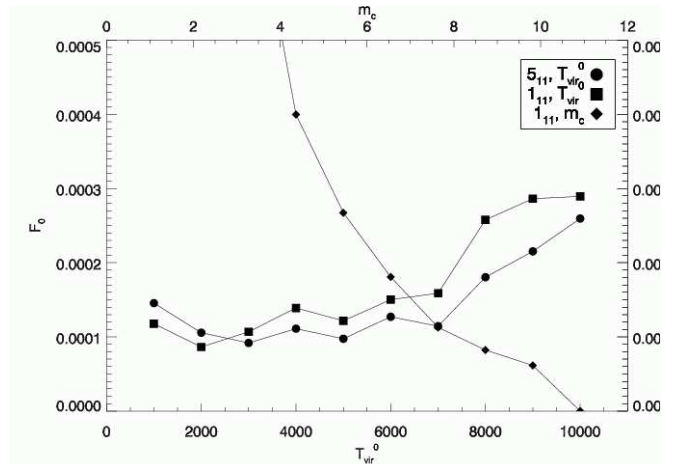


FIG. 5.— Variation of  $F_0$  with  $T_{vir}^0$  for trees of  $M_h = 1$  and  $5 \times 10^{11} M_\odot$  (filled circles and squares, respectively) and an IMF with  $m_c = 10$ ,  $\sigma = 1.0$ . The filled diamonds show  $F_0$ , divided by 10, for variations in  $m_c$  as shown on the top axis, and with fixed  $\sigma = 1.0$ . Variations due to statistical noise and systematic uncertainties in  $M_h$  and  $T_{vir}^0$  are overwhelmed by variations with IMF parameters.  $F_0$  is therefore a robust indicator of the IMF.

$10^{-3.5}$  underproduces them. For  $Z_{crit} \leq 10^{-4.5}$ , the model MDF converges to a single curve because adding stars with extremely low  $[\text{Fe}/\text{H}]$  adds very little to the cumulative total. The MDF is matched reasonably well by  $Z_{crit} \simeq -4.0$ , or roughly the lowest metallicity present in the RN91 MDF. The MDF appears smooth down to  $[\text{Fe}/\text{H}] = -3.8$ , and this smooth distribution can be explained by the same model parameters and IMF that match the other observables. Thus it seems that the observations require  $Z_{crit} \leq 10^{-3.8}$ . Indeed, the IMF and  $Z_{crit}$  are intimately connected, because the number of low-mass stars below  $Z_{crit}$ , that can contribute to the cumulative distribution, depends on the IMF at  $Z < Z_{crit}$ . Unless a clear-cut break is seen in future updates to the observed MDF,  $Z_{crit}$  will probably not be constrained in this fashion. However, it can be constrained along with all the other model properties, i.e., if an IMF can be independently determined by  $F_0$  and reionization,  $Z_{crit}$  can be inferred. This test would also require much better statistics in the low- $[\text{Fe}/\text{H}]$  bins, where currently there are only a handful of stars. Because of the dearth of data below  $[\text{Fe}/\text{H}] \lesssim -3$ , it seems the critical metallicity for normal star formation has not yet been detected.

The rigid limit at a single  $[\text{Fe}/\text{H}]$  is a direct consequence of the assumption that there is a single  $Z_{crit}$ . Models by Santoro & Shull (2005) suggest that the critical metallicity can depend on both the particular mix of metals (Si/C rich vs. Fe rich) and the initial temperature and density conditions of collapse. These additional factors can blur out the single  $Z_{crit}$  assumed here, and may in fact yield a range of critical metallicities that extends above the lowest- $[\text{Fe}/\text{H}]$  star seen in the halo. Future work will endeavor to incorporate a broader range of assumptions about  $Z_{crit}$  and connect them to observations and detailed theory.

## 5.2. IMF Constraints from Reionization

The second major constraint on the IMF is that the ionizing photon budget must be sufficient to provide

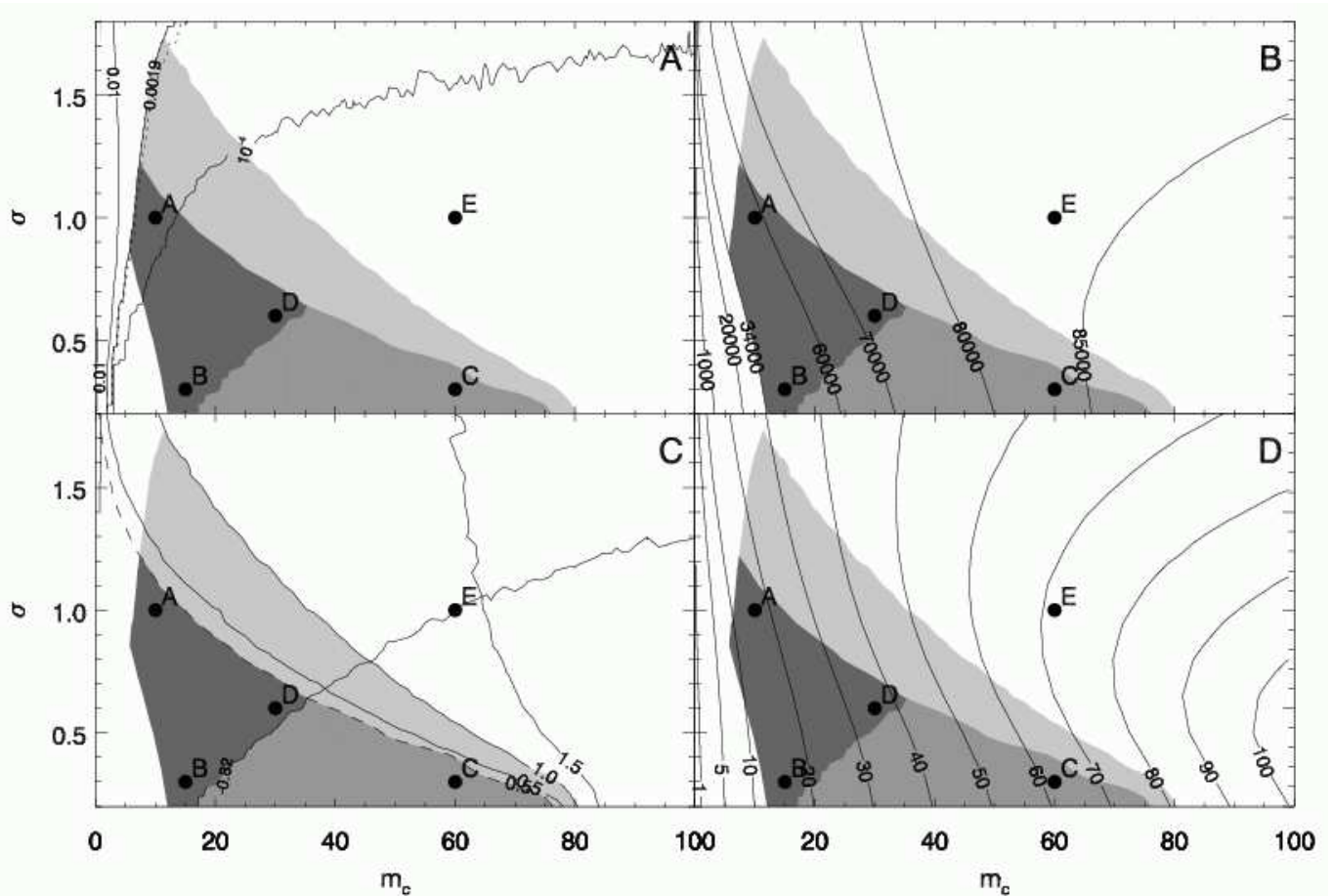


FIG. 6.— Observational constraints on the parameters for a primordial IMF. Each panel shows contours for an individual constraint, while the shaded regions that meet all constraints are the same in all panels. Panel A: Contours of  $F_0$  for log-normal IMF parameters.  $F_0 \leq 0.0019$  requires  $m_c \gtrsim 4 M_\odot$ . Panel B: Contours of constant ionizing efficiency  $\gamma_0$  for  $Z = 0$  stellar atmosphere models from TSV03. Panel C: Solid contours show constant  $[\text{Zn}/\text{Fe}]$  from 8 - 40  $M_\odot$  that is required for the given IMF to yield average  $[\text{Zn}/\text{Fe}] = 0.3$  in the metal-poor stars from the Cayrel et al. (2004) sample. Dashed contours show constant iron production ratio from VMSs,  $F_{VMS}$ . Above the contours  $[\text{Zn}/\text{Fe}] = 1.0$  and  $F_{VMS} = 0.9$ , VMSs dominate the Fe production so much that unsuitably large Zn excess is required from massive stars. Also shown with a dashed line is the contour of constant  $F_{VMS} = 0.5$ , or one-half of the total iron budget coming from VMSs. See text for discussion. Panel D: Mean stellar mass of a log-normal IMF with the given parameters. This quantity is a derived output of the model and not an independent constraint.

a high optical depth to reionization,  $\tau_{es} \geq 0.1$ . To meet this constraint, the TVS04 models suggest that  $\gamma_0 \geq 34000$  is needed. This is a somewhat model-dependent constraint on the IMF, because it involves a number of poorly understood astrophysical parameters, such as the escape fraction of ionizing radiation from early galaxies, and the disposition of “minihalos” with  $T_{vir} < 10^4$  K. As argued in § 4.2,  $\gamma_0 \geq 34000$  is needed to give  $\tau_{es} \geq 0.1$ , the smallest value within the  $1\sigma$  confidence interval of the first-year *WMAP* data. Panel B of Figure 6 shows contours of  $\gamma_0$  in the IMF parameter space, using the mass-dependent  $\gamma_0$  results in Figure 2 of TVS04. Clearly  $\gamma_0 \geq 34000$  requires an IMF skewed to high mass, such that the same general range of low  $m_c$  and small  $\sigma$  excluded by  $F_0$  is also excluded by  $\gamma_0$ . Together,  $F_0$  and  $\gamma_0$  constrain the IMF to  $m_c \geq 6 M_\odot$ . IMFs with much higher  $\gamma_0$  are permitted, including very efficiently ionizing IMFs that could give  $\tau_{es} \gtrsim 0.14$ . In this sense the requirement that  $\tau_{es} \geq 0.10$  ( $1\sigma$  confidence from *WMAP*) is conservative. Meeting the  $\tau_{es}$  constraint seems to require at least some star formation in minihalos with  $T_{vir} \leq 10^4$  K, which complicates some of the other

IMF limits (see also Section 5.5 for more discussion).

### 5.3. IMF Constraints from Detailed Nucleosynthesis

Additional, and more model-dependent, constraints on the IMF come from the detailed abundances seen in metal-poor stars. As argued in TVS04, the presence of the r-process elements in the EMPs do not allow the early budget of iron to be provided exclusively by PISNe, which have no r-process (HW02; TVS04). TVS04 also argued that the early budget of Fe could not be dominated by the peculiar nucleosynthetic signature of VMSs, which show a strong odd-even effect and deficits in some Fe-peak elements (particularly Zn). That paper did not, however, attempt to place quantitative constraints on the Fe budget that could have come from VMSs. This boundary can be defined precisely only if detailed models using Type II and PISNe yields are fitted with the observed samples for the full range of IMF parameters, using some type of goodness-of-fit metric. However, this analysis would require a complete “basis set” of mass- and metallicity-dependent yields for metal-free Type II SN, which does not exist (especially for core-collapse SNe

models, which do not spontaneously explode and have many tunable parameters). Because extracting detailed empirical yields directly from the data on metal-poor stars is a goal of the final model, it is best to avoid direct reliance on the theoretical yields where possible. Despite this desire, there is probably no reasonable alternative for constraining the upper right corner of the IMF parameter space, where VMSs overwhelmingly dominate the mass and iron budget. This portion of parameter space easily meets the  $F_0$  and  $\gamma_0$  limits, leaving nucleosynthesis and future high-redshift galaxy searches as the remaining possible constraints. For the purposes of this study it is sufficient to establish some conservative upper limit to the contributions of VMSs to early chemical evolution. This constraint implicitly assumes that all SNe yields are retained in their parent halos. This assumption is likely to be violated in minihalos with  $T_{vir} \lesssim 10^4$  K, so if they prove necessary to match the overall dataset, these limits will need to be reevaluated.

When PISNe yields are compared against the stellar abundance data, either by integration over an IMF (HW02) or for individual masses (TVS04), the most discrepant element is zinc. PISNe produce very little Zn in an  $\alpha$ -rich freeze-out, and that only in the upper mass range. Thus high Zn yields must be produced from 8 – 40  $M_\odot$  for the IMF-weighted mass yields to match the data, which for the Cayrel et al. (2004) sample shows  $\langle [Zn/Fe] \rangle = 0.3$ . A possible constraint comes from asking what typical Zn yield is needed for 8 - 40  $M_\odot$  to compensate for PISNe and match the data with a given IMF. The solid contours in panel C of Figure 6 mark the  $[Zn/Fe]$  excess that is needed, uniformly across the range 8 - 40  $M_\odot$ , to overcome the strong  $[Zn/Fe]$  deficit of PISNe and still give a mean  $[Zn/Fe] \approx 0.3$  for stars with  $[Fe/H] \leq -2$ . IMFs in the upper right corner require very high Zn excess,  $[Zn/Fe] \gtrsim 1.0$ . To constrain the IMF, I adopt  $[Zn/Fe] \leq 1.0$  as a conservative limit. This constraint on the Fe budget from VMSs places a constraint on how top-heavy the IMF can be that is complementary to  $F_0$ . The IMF cannot occupy any region above the line which roughly runs from (20, 1.5) through (35, 1.0) to (60, 0.5). This still leaves a lot of parameter space, but has at least provided a key constraint at the upper end, complementary to the  $F_0$  constraint at the lower end of the IMF.

This  $[Zn/Fe]$  limit is called conservative for two reasons. First, this Zn excess is higher than that produced in typical published models of core-collapse supernova nucleosynthesis. Umeda & Nomoto (2002) show that with no mixing and/or fallback to enhance the elements above Fe,  $[Zn/Fe] \lesssim 0.0$ . Their models that include mixing and fallback with the explicit purpose of better matching the Fe-peak elements (Cayrel et al. 2004) have  $[Zn/Fe] = 0.3 - 0.5$ , with a maximum of +0.5 produced by a supernova that explodes with  $E = 30 \times 10^{51}$  erg (Umeda & Nomoto 2005). The zero-metallicity models of Woosley & Weaver (1995) all have  $[Zn/Fe] \lesssim 0.0$ . Thus even assuming  $[Zn/Fe] = 0.5$  for all 8 - 40  $M_\odot$  SNe strains the existing models to their limits. In this sense, placing the limit at  $[Zn/Fe] \leq 1.0$  is conservative. Second,  $[Zn/Fe] \leq 1.0$  for 8 - 40  $M_\odot$  limits the Fe budget contributed by PISNe rather generously to  $f_{VMS} \leq 90\%$ . This limit is called generous because it is probably more than can reasonably be accommodated by the observed abundances

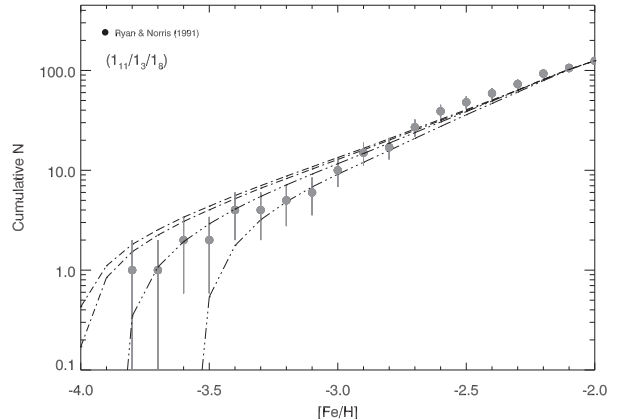


FIG. 7.— Cumulative MDF for RN91 and a (1<sub>11</sub>/1<sub>3</sub>/1<sub>8</sub>) tree and  $Z_{crit} = -5.0, -4.0, -3.8, -3.5$  marked with lines, from top.  $Z_{crit}$  appears to be  $< -3.5$  and fits best for  $Z_{crit} = -3.8$  (the most metal-poor star from RN91 has  $[Fe/H] = -3.7$ ) but is otherwise not well constrained by the few points below  $[Fe/H] = -3$ .

in the metal-poor stars. HW02 note that a power-law IMF with Salpeter slope (which produces  $\sim 50\%$  of its Fe with VMSs given the adopted SN mass ranges) has too pronounced an odd-even effect. This tighter constraint is displayed in a dashed contour in panel C of Figure 6 and adopted as a more realistic constraint on the IMF. A 10% percent contribution from VMS is probably still more realistic given their pronounced odd-even effect. There are two reasons for setting this limit conservatively. First, deriving more quantitative, and more restrictive, constraints on  $F_{VMS}$  based on some goodness-of-fit-test would require undesirable reliance on the detailed theoretical yields. Second, as noted by HW02, Zn may have an alternative production site beyond the  $\alpha$ -rich freeze-out at the higher masses. There may be a neutrino-driven wind that could leave an important contribution to Zn production and permit lower  $[Zn/Fe]$  from massive stars (8 - 40  $M_\odot$ ). This feature has not been modeled extensively for massive stars or VMSs, so it remains speculative. Of course, this would leave the severe odd-even effect, but this is less quantifiable. In light of these two motivations the conservative limit on  $[Zn/Fe]$  seems reasonable. Thus weak-VMS IMFs are permitted by the existing data and conservative assumptions about intrinsic yields.

There is an additional constraint from detailed nucleosynthesis that is more speculative but potentially even more powerful than the observed ratios of iron-peak elements for constraining the IMF - the frequency of r-process enrichment observed in metal-poor stars. This constraint is more speculative because it relies on an assumption that r-process elements are uniquely associated with a narrow range of the IMF, between 8 and 12  $M_\odot$ . It is potentially more powerful for exactly that same reason. The basic idea is possible because the r-process elements (here represented by barium) cannot be produced in PISNe, and are thought to be associated with core-collapse SNe in the range 8 - 12  $M_\odot$ . Thus we can use the observed frequency of r-process enrichment at  $[Fe/H] < -2$  as leverage on the shape of the IMF.

This simple model for r-process enrichment that follows

in the spirit of the phenomenological model of Fields, Truran, & Cowan (2002). The sample starts with the HERES sample of Barklem et al. (2005), and is first culled to include only their 228 stars from the HE survey. I include only stars with  $[\text{Fe}/\text{H}] < -2.5$ , below which it is believed that all Ba comes from the r-process (Truran et al. 2002). In this remaining sample of 146 stars, 119 (82%) show detected Ba at  $[\text{Ba}/\text{Fe}] > -2$ . To test this against model IMFs, chemical evolution histories for low-metallicity stars are constructed, allowing for 10 SN progenitors (see § 6.1). Iron yields are assumed as given above for the Type II (8 - 40  $M_{\odot}$ ) and PISNe (140 - 260  $M_{\odot}$ ) mass ranges. Over the range 8 - 12  $M_{\odot}$ , SNe are assumed to produce Ba in the highest observed pure r-process ratio relative to Fe,  $[\text{Ba}/\text{Fe}] = 1.5$ . This high ratio, which is only observed for rare (r-II; Barklem et al. 2005) objects, represents an extreme high value for the r-process Ba yield of a single SNe and so helps set a conservative limit on the iron-rich/r-process poor contribution at the high end of the IMF.

The results of this test appear in Panel C of Figure 6. The contour labeled “0.82” separates IMFs which have a suitable ratio of r-process to iron progenitors (above the contour) from those that produce too much iron and not enough r-process enrichment. The parameter space excluded by this test is reproduced in the medium gray shade in the other panels.

This is the most model-dependent of the constraints placed on the IMF, because it assumes that r-process enrichment is produced only by stars with 8 - 12  $M_{\odot}$ . This mass range is favored by theoretical models of the r process in supernovae (Woosley et al. 1994; Truran et al. 2002) but is still unconfirmed by observation. If the r process occurs in SNe across the full range (8 - 40  $M_{\odot}$ ), r-process progenitors are quite numerous and push the 82% constraint out of the interesting IMF parameter space. For this reason this test is only a tentative constraint and continue with an IMF test case that lies in the region excluded by this uncertain, but potentially very powerful test.

These constraints from detailed nucleosynthesis exploit the unusual behavior of PISNe from very massive stars with 140 - 260  $M_{\odot}$ . At the high mass end, these stars eject up to 40  $M_{\odot}$  of iron and correspondingly large masses of other detectable elements (HW02). However, as discussed below in § 5.5, if these stars form predominantly in minihalos with  $T_{\text{vir}} \lesssim 10^4$  K, they may also disrupt their parent halos with energetic supernovae, and therefore not leave their nucleosynthetic products eligible to enrich later generations of star formation. While minihalos are not required to match the observed MDF and  $F_0$  constraints, they may in fact be required to form stars efficiently to meet the reionization constraints of *WMAP* or future CMB results. This section has implicitly assumed that these VMSs form in  $T_{\text{vir}} > 10^4$  K halos in addition to minihalos, and that their ejected metals remain bound. Thus the nucleosynthesis constraints on the upper end of the IMF, discussed here, and the reionization constraints may not be achievable simultaneously. Minihalos are discussed more thoroughly below in Section 5.5.

#### 5.4. IMF Test Cases

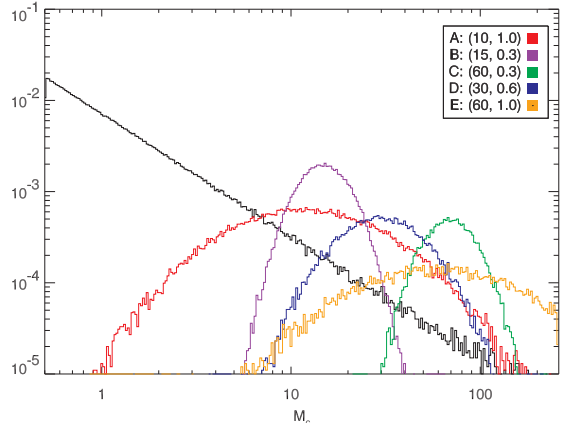


FIG. 8.— The possible log-normal IMFs drawn from Figure 6, compared with a power-law IMF of Salpeter slope,  $\alpha = -2.35$ , all normalized to have the same total mass  $10^6 M_{\odot}$ . The best-fitting IMFs are all sharply peaked in the range 12 - 70  $M_{\odot}$ . See the discussion in the text for details.

The various constraints in combination suggest an IMF for the first stars that is restricted to the dark shaded area in Figure 6. This IMF is restricted to  $m_c = 6 - 35 M_{\odot}$ , with  $\sigma \approx 0.3 - 1.2$  and mean mass  $\langle M \rangle = 8 - 42 M_{\odot}$ . Within this permitted range, there are not yet detailed constraints that can discriminate the parameters still further. I define five IMF test cases for further examination of their detailed properties and consequences. These are labeled IMF A (10, 1.0), B (15, 0.3), C (60, 0.3), D (30, 0.5) and E (60, 1.0). These represent, respectively, two low- $m_c$  models which are only as top-heavy as they need to be, but with different widths, a high-mass model sharply peaked at  $\langle M \rangle = 70 M_{\odot}$  (perhaps excluded by r-process abundances), a model intermediate between A, B, and C, and then E, an extreme top-heavy IMF useful for exploring the importance of feedback on minihalos and the feasibility of the  $[\text{Zn}/\text{Fe}]$  constraint. These test cases are shown in the left panel of Figure 8 compared against the power-law Salpeter IMF.

The MDF provides a possible test of the IMF cases. The results of these comparisons appear in Figure 9. IMFs A and B provide the overall best fit. IMF B has a strong deficiency of VMP and EMP stars relative to the RN91 MDF, while IMFs C and E have an excess. This “bump” feature is caused by the strong deficiency of stars that produce a nucleosynthetic signature (8 - 40  $M_{\odot}$ ) relative to those that do not (40 - 140  $M_{\odot}$ ). Both of these IMFs (C and E) are potentially excluded with detailed nucleosynthetic results presented above and they also produce poor fits to the overall MDF. For these reasons we disfavor these IMFs. However, these MDF results are not decisive for determining the IMF because of the poor statistics in the data below  $[\text{Fe}/\text{H}] \sim -2.5$ . Improvements in the sample size expected from future large surveys of Galactic halo metal-poor stars have the potential to tighten IMF constraints based on the Galactic halo MDF.

Different star formation histories for metal-free stars can also help discriminate the IMF test cases. An IMF that is more top-heavy, and which places more mass into the 40 - 140  $M_{\odot}$  range of stellar mass that does not

produce a nucleosynthetic signature, will take longer to produce a fixed overall enrichment and so should form metal-free stars for a longer time in each halo. This effect could potentially be detected at high redshift. It is expected to be particularly severe for the high-mass cases C and E, which peak between the mass ranges of Type II SN and PISNe. As the right panel of Figure 9 shows, the metal-free star formation histories of a  $(5_{11}/1_3/1_8)$  tree are not significantly different for the cases A, B, and D, with variations of less than a factor of two at  $z = 10 - 20$ . But for the more top-heavy cases C and E the metal-free star formation rate is quite different, and could be used as an IMF indicator. These cases may be excluded by the r-process elements and  $[\text{Zn}/\text{Fe}]$  and produce a noticeably poor MDF, but illustrates the key point that observed star formation histories in the early universe can now be connected explicitly to Galactic chemical evolution and may yield important information on the IMF.

Lucatello et al. (2005) followed another nucleosynthetic approach to constraining the early IMF. They used the  $[\text{Fe}/\text{H}] \approx -2$  onset of s-process elements from AGB stars to constrain the IMF to have  $\langle\sigma\rangle = 1.18$  and  $m_c = 0.79$  ( $\langle M \rangle = 1.8 M_\odot$ ). When used in this model for  $Z < Z_{crit}$ , their proposed IMF gives a Population III number fraction  $F_0 = 0.2$ , far above the observed constraint. This discrepancy is probably related to the fact that their model has no leverage on high-mass stars. This nucleosynthesis model does have such leverage. The permitted IMFs here, with  $m_c \gtrsim 10$  and  $\sigma \sim 1.0$ , easily satisfy the constraints imposed by their analysis of s-process elements, and so confirm their suggestion of a more massive primordial IMF, but skewed even further toward massive stars.

### 5.5. Behavior of “Minihalos”

The fiducial  $(5_{11}/1_3/1_8)$  tree contains approximately 1 million total progenitor halos extending down to  $T_{vir} = 10^3$  K. Halos between  $10^3$  K and  $10^4$  K are generally termed “minihalos”, and are thought to cool only with molecular hydrogen, while more massive halos can cool at least partly by emitting recombination emission of H, which is ionized above  $T \approx 10^4$  K. Being small in mass ( $M \simeq 10^5 - 10^6 M_\odot$  at  $z \sim 10 - 30$ ), minihalos also may be easily ionized by main-sequence massive stars, and even disrupted completely by energetic supernovae. This model has, up to this point, treated minihalos as “closed boxes” which do not experience ionization or mechanical feedback. The strongest constraint on the primordial IMF,  $F_0$ , does not depend on the assumed minimum virial temperature in the tree (see Figure 5), but the other constraints do depend somewhat on the behavior of minihalos, and thus may be modified by the feedback effects of massive stars. This section develops some limiting cases of radiative and mechanical feedback to assess the sensitivity of the IMF constraints to these processes. These feedback effects will be more fully explored and connected to a Galactic chemical evolution model in future work.

First I consider the local effects of ionization by massive stars. It is possible for massive stars to produce H II regions that completely ionize the gas bound to minihalos. This process has been studied by Kitayama et al. (2004) over a range of minihalo masses and assumptions about stellar mass. They derived a critical halo

mass below which a minihalo is completely ionized for a given stellar mass (see their Equation 14). This feedback mechanism removes from the gas reservoir the entire gas mass of halos that possess a massive star sufficient to completely ionize its gas, according to the Kitayama et al. criterion. This assumption represents an extreme, since it does not return this gas to the reservoir as if it had recombined and cooled at a later time (this time is estimated by Kitayama et al. at a few tens of millions of years). Returning the recombined gas to the reservoir would allow subsequent metal-enriched star formation (with metals ejected by the same massive star that ionized it), so including feedback increases  $F_0$  as much as possible by inhibiting star formation in small halos after the first, metal-free generation. The overall increase in  $F_0$  is 20% or less over its value in a tree with no feedback. The corresponding change in the  $F_0$  constraint on the IMF is shown with the dashed contour in panel A of Figure 6, which marks the contour for  $F_0 = 0.0019$  including a 20% increase in  $F_0$  to account for radiation feedback. This effect is modest because it touches only a small number of halos and a small fraction of the total gas budget. Future work will need to focus on more detailed treatments of this feedback mechanism to implement cases in between the fiducial model and this extreme modification, and to assess its overall importance to chemical evolution.

The other possible feedback mechanism which can affect chemical evolution is the mechanical disruption of small halos by supernovae. PISNe are particularly good at disrupting small halos ( $M \lesssim 10^7 M_\odot$ ) as they release up to  $\sim 10^{53}$  erg per event (HW02). This feedback mechanism violates the assumption of a closed box from which gas and metals do not escape. Because this effect is preferentially caused by PISNe at the higher mass end, it can invalidate the limits placed above on  $[\text{Zn}/\text{Fe}]$  and  $[\text{r}/\text{Fe}]$ , which implicitly assume that the high iron yields of high-mass PISNe are retained in their parent halos and dilute the Zn and r-process yields of core-collapse SNe. Thus it is important to assess the potential effect of this feedback mechanism on the limits of interest, the IMF constraints, and on Galactic chemical evolution in general.

A simple prescription expresses mechanical feedback. VMSs are allowed to form as usual, but when one of them experiences a PISN, a check is done to see whether the total energy of the supernova (seen in HW02 Figure 1) is larger than the binding energy of the gas in the parent dark matter halo. If so, this gas reservoir is permanently removed from the tree and assumed to reside in the diffuse IGM, where it is no longer tracked. The effect of this feedback mechanism on  $F_0$  has already been taken into account as ionization, since SNe that disrupt their parent halos have already ionized them. The more top-heavy IMFs disrupt up to two third of all minihalos in the tree. The main effect of this SNe “blowout” is to remove from the available reservoir of metals the very high iron yields that dilute the products of core-collapse SNe and allow the limits from detailed nucleosynthesis placed above in Section 5.3. In the presence of feedback, these limits are easily achieved and the upper end of the IMF is difficult to constrain because it leaves no detailed nucleosynthetic signature. If star formation begins in earnest in halos with  $T_{vir} \lesssim 10^4$  K, a wide range of weak-VMS IMFs are formally permitted. However, even accounting



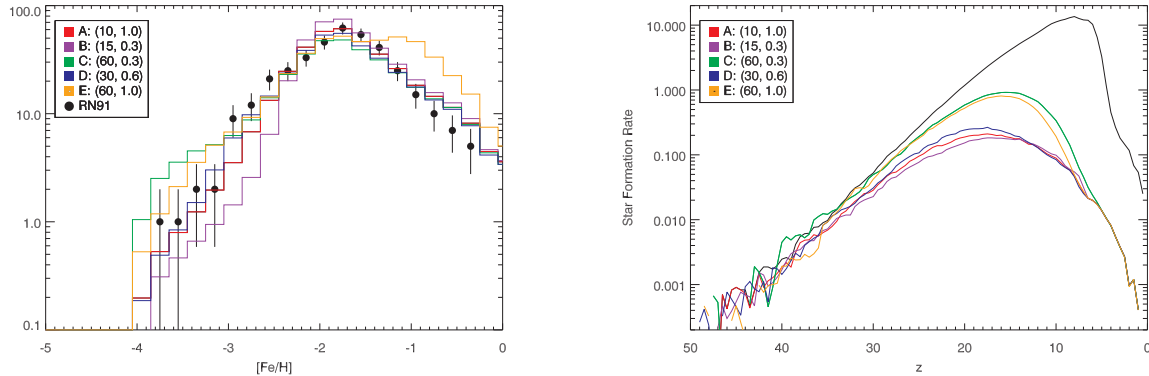


FIG. 9.— Left panel: Comparison of MDFs for the five IMF test cases, normalized to the same total number of stars as in the complete RN91 MDF. Cases A and D yield reasonable fits, but cases C and E show a strong “bump” feature just above  $Z_{crit}$  that is not seen in the data, while case B is deficient in EMP stars. Models sharply peaked with  $m_c = 10 - 30 M_\odot$  are favored by the overall dataset. Right panel: Comparison of metal-free SFRs for these different IMFs, which may be distinguishable in the future from the level of metal-free star formation activity observed at high redshift. Model IMFs C and E have the highest mass in the 50 - 140  $M_\odot$  range, so they result in the highest overall  $Z = 0$  SFR. The black curve shows the overall SFR (at all metallicities). This quantity is not sensitive to the IMF and is represented here by IMF case A.

for PISNe feedback, these IMFs produce inferior fits to the MDF (see Figure 9). Nevertheless, these effects may make it difficult to uncover evidence of the absence of VMSs from the IMF.

While SNe feedback complicates two possible nucleosynthetic limits on the early IMF, it opens another potential avenue for detailed constraints at the high-mass end. By removing from the gas reservoir material which is otherwise eligible for later star formation, and by affecting potentially more than one-half of low-mass branches in the tree, this mechanical feedback has a strong effect on the total budget of ionizing photons that can escape and reionize the IGM. Preliminary calculations suggest that for (50, 1.2), which produces 96% of its Fe with VMSs and so lies outside the  $[Zn/Fe]$  constraint from above, loses 30% of its cumulative budget of ionizing photons (up to  $z = 10$ ) to halo disruption, thereby dropping from  $\gamma_0 = 82600$  to an effective value of 57800. This value still meets the fiducial constraint of  $\gamma_0 \geq 34000$ . This reduction is less than expected given that more than 2/3 of the minihalo branches in the tree terminate in a PISN. Future models that treat reionization and chemical evolution in detail will need to fully explore this feedback process.

## 6. GENERAL RESULTS FROM THE MODEL

This section describes some general results derived from the chemical evolution model that do not depend on or relate directly to the IMF, which has been the focus of the paper. These results include information from detailed chemical evolution histories of metal-poor stars, the end of the first stars epoch.

### 6.1. Results on Detailed Nucleosynthesis

A given merger tree with chemical evolution allows for calculation of the chemical histories of individual metal-poor stars, for the first time in their proper context. These histories include the number, masses, metallicities, and supernova times of all progenitor SNe. This information is critical to properly interpreting the relative element abundances in metal-poor stars (Beers & Christlieb

2005). There are two approaches to using this information to understand the SNe yields of the first stars. The first is to apply a “basis set” of theoretical yields to the calculated distribution of progenitor masses and metallicities, and then compare the calculated relative abundances to the data to adjust the IMF parameters and optimize the fit. The second is to attempt to extract intrinsic yields directly from the data empirically, with assistance from a chemical evolution model. The former approach, which is commonly used in studies of the metal-poor stars, is complicated by the fact that there is really no suitable “basis set” of theoretical supernova yields. Inspection of the yield tables in Woosley and Weaver (1995) shows that theoretical yields vary dramatically with mass and metallicity, and sparsely sample the available ranges in these variables. There are also significant uncertainties associated with the choice of supernova energy and mass cut between the compact remnant and the ejecta. Recent models (e.g. Umeda & Nomoto 2005) have introduced additional parameters associated with mixing of material across the mass cut and a wider range of explosion energies, in an effort to better match the observed Fe-peak elements in Galactic EMPs. Finally, model Type II core-collapse SNe still do not spontaneously explode - the SN energy must still be introduced by hand. These factors taken together mean that attempting to assemble a true “basis set” of model yields is quite difficult - no single group or study has densely sampled the full parameter space needed to map out the range of masses and metallicities probed here and in the data. Also, this approach would introduce many more tunable parameters into the model with sure loss of confidence in the results.

For these reasons I adopt the latter approach, namely, to attempt to extract information, and perhaps detailed yields, directly from the data with assistance from the chemical evolution model. This approach complements the direct modeling of observed abundance patterns by potentially revealing new trends that result from the underlying processes of chemical evolution. This method is enabled by the detailed chemical evolution histories

available from the model presented here. Figure 10 shows detailed results for the IMF test-case A in a  $(5_{11}/1_4/1_8)$  tree, and shows the power of these models to interpret the metal-poor stellar abundance data in the proper context. Panel A shows the overall MDF for this fiducial tree. Panel B shows, for all the metal-poor stars in the tree, the fraction of their progenitors that were metal-free stars. Panel C shows the mass distribution of progenitor SN for each metal-poor star, and panel D shows the number of progenitors for each star. In the latter three panels, the mean quantity in 0.2 dex bins is plotted with a square, and the  $1\sigma$  scatter in that quantity is plotted with error bars.

A number of important results appear in this figure. First, the model is constructed to preserve a great amount of useful information about the history of chemical enrichment in the model Galaxy, most importantly the mass and metallicity distribution of SNe precursors for metal-poor stars for a given parameter set and tree realization. Second, combining the results of panels B and D, I find that below  $[\text{Fe}/\text{H}] \sim -3$ , EMP stars have 1 - 10 SNe precursors, all of which are metal-free. In fact, the average  $[\text{Fe}/\text{H}] \sim -4$  (UMP) star had exactly one metal-free precursor. This removes the dependence of the observed abundances on precursor metallicity and leaves only precursor mass as a variable. Thus the variation of  $[\text{Zn}/\text{Fe}]$  with  $[\text{Fe}/\text{H}]$  below  $[\text{Fe}/\text{H}] = -3$  (Cayrel et al. 2004) may be explained simply as an effect of SN precursor mass, with more massive, short-lived precursors,  $M \simeq 30-40 M_{\odot}$ , coming in first at  $[\text{Fe}/\text{H}] \lesssim -4$ , followed by longer-lived precursors of  $8-10 M_{\odot}$  only at  $[\text{Fe}/\text{H}] \sim -3$ . Put another way, the mean mass of precursors declines from  $\sim 35$  to  $\sim 15 M_{\odot}$  over the range  $[\text{Fe}/\text{H}] = -4$  to  $= 2$ . Finally, the predicted number of precursors per metal-poor star, and their mass and metallicity distribution, can be used to assess the scatter in observed  $[\text{X}/\text{Fe}]$  ratios. This conclusion has interesting implications for the interpretation of observed r-process abundances that will be explored in a future paper.

These key results represent a major step toward the final goal of extracting intrinsic yields of the first SNe directly from the data. This study has developed the framework needed to perform this analysis within the proper context of galaxy formation. Future work will focus on exploring the full range of possibilities in parameters, on understanding the systematic errors, and on assessing the volume of data and level of data quality needed to give satisfactory results.

### 6.2. End of the First Stars Epoch

There are no known locations in the local universe where metal-free gas is known to exist. Intensive efforts to discover galaxies at  $z > 6$  (the end of reionization) have not yet turned up any galaxies that are clearly metal-free, or even known to have  $[\text{Fe}/\text{H}] \lesssim -2$ , the lowest metallicity seen in the local universe. Thus metal-free star formation must have been curtailed at some point in the early universe, probably in the first 1 Gyr after the Big Bang. In the absence of any observational information about metal enrichment of galaxies before  $z = 6$ , theorists have approached the problem by trying to estimate the time needed for galaxies to enrich themselves, or neighboring galaxies, using simulations and semi-analytic models in a similar spirit to the

one presented here.

If the metal enrichment history of the Galaxy’s halo is typical, star formation is already substantially enriched with metals even by  $z = 20$ . According to Figure 9, for IMFs A, B, and D, only 10 - 20% of star formation is still metal-free at  $z = 20$ , where the total rate of truly metal-free star formation in the Galaxy’s history peaks at  $0.2 M_{\odot} \text{ yr}^{-1}$ . By  $z \sim 6$ , metal-free star formation has declined to 3% of the total star formation rate in halo progenitors. This metal-free star formation is isolated to small “leaf” halos which have just virialized, not distributed throughout halos that are also forming metal-enriched stars. If the Milky Way halo is a representative sample of high-redshift star formation, there is a quite low probability of finding a truly metal-free star-forming galaxy at  $z \sim 6$ , owing to the self-enrichment of halos by local star formation.

Figure 11, which shows star formation times and metallicities for a  $(5_{11}/1_3/1_8)$  tree, showing the spread in times for a single  $[\text{Fe}/\text{H}]$ , or the spread in  $[\text{Fe}/\text{H}]$  at a given time. Clearly time and metallicity are not perfectly correlated and low-metallicity stars form throughout the history of Galactic halo formation. In the lower panel, the curves show the fraction of star formation in different metallicity ranges as a function of time since the onset of star formation in the tree. For the first 10 Myr, star formation is exclusively metal-free (black curve), but by 30 Myr it has become only 20% of all star formation.

By relating high- $z$  star formation rates directly to Galactic chemical evolution, this model can provide additional unique constraints on the nature of the earliest stellar populations. Future work will focus on expanding the chemical evolution model applied here to the Galaxy to a population of galaxies at an arbitrary redshift in population syntheses that can be compared directly to high-redshift data and to the Galactic halo stars.

## 7. DISCUSSION

By connecting chemical evolution to Galaxy formation, this model has placed meaningful constraints on the mass function of the first stars using a broad range of observational information. I now consider how these constraints might improve with additional data, and how theory might guide future experiments.

The samples of metal-poor Galactic halo stars are expected to grow dramatically in the next decade owing to systematic surveys dedicated to finding and studying large stellar populations in the outer galaxy. The SEGUE extension to the Sloan Digital Sky Survey<sup>1</sup> will discover up to 20000 stars with  $[\text{Fe}/\text{H}] < -2.0$ , 2000 with  $[\text{Fe}/\text{H}] < -3.0$ , 200 with  $[\text{Fe}/\text{H}] < -4.0$ , and a few stars with  $[\text{Fe}/\text{H}] \sim -5$  to  $-6$ , should they exist. SEGUE will construct the sample and estimate stellar parameters and  $[\text{Fe}/\text{H}]$ . These stars can then be studied at high resolution and good S/N with 8 m class telescopes to read from them the mass assembly and chemical evolution history of the Galaxy. Another such survey is the WFMOS project, which is planned to obtain high-resolution spectra of 1 million stars with a 1000-fiber optical spectrograph mounted on the Subaru telescope<sup>2</sup>. This survey is also directed at the earliest phases of chemical evo-

<sup>1</sup> <http://www.sdss.org>

<sup>2</sup> <http://www.gemini.edu/science/aspden/wfmoss-sciobj.pdf>

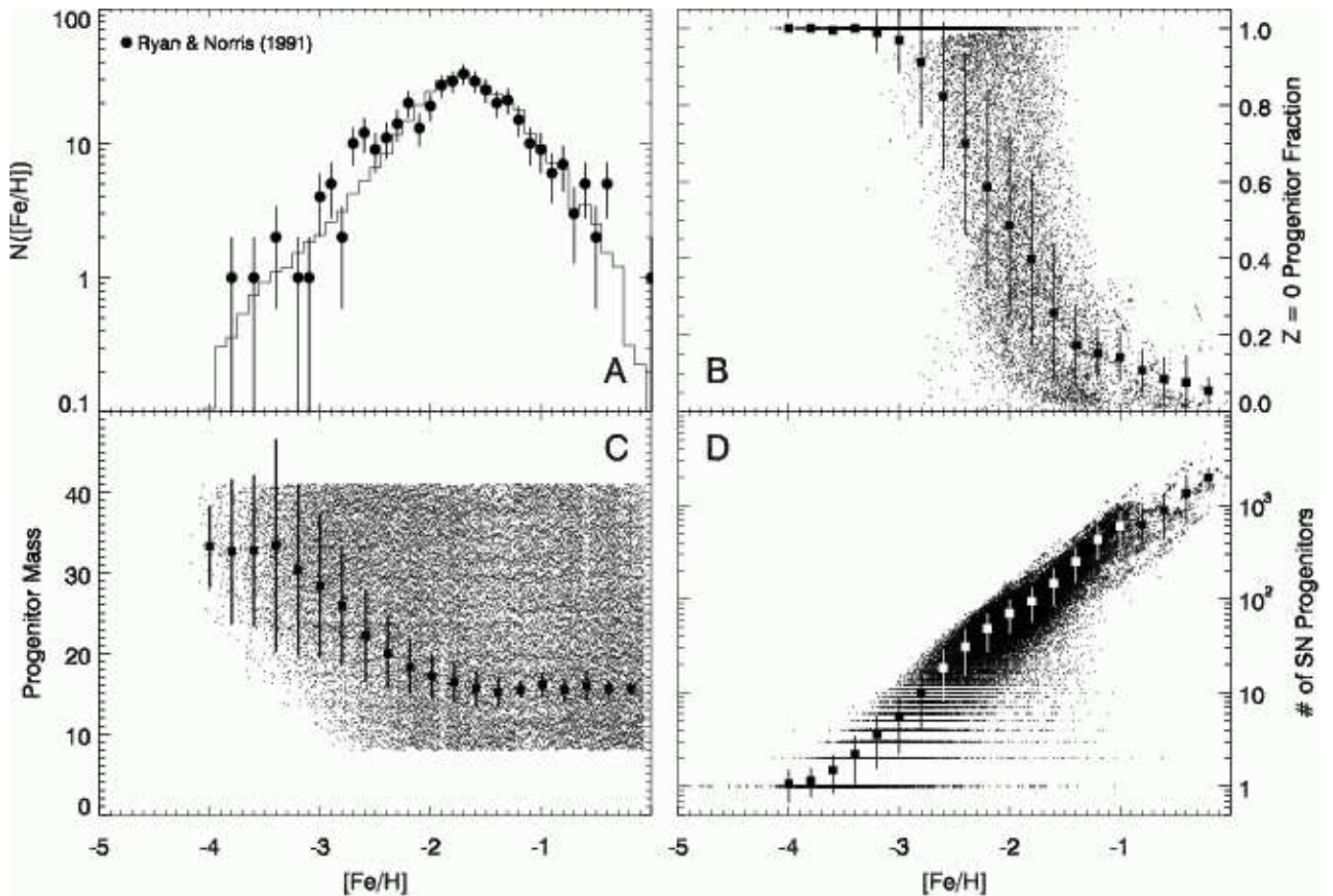


FIG. 10.— Detailed chemical evolution histories for model metal-poor stars. Panel A: MDF calculated for a single ( $5_{11}/1_4/1_8$ ) tree, IMF case A, and  $Z_{crit} = -4$ . Panel B: As a function of final stellar metallicity, the fraction of its SN progenitors that were metal-free. Squares mark the mean in 0.2 dex bins, with  $1\sigma$  scatter shown by error bars. Between  $[\text{Fe}/\text{H}] = -3$  and  $[\text{Fe}/\text{H}] = -2$ , this fraction drops dramatically from 1 to  $< 10\%$ . Panel C: As a function of final metallicity, the distribution of progenitor masses for each metal-poor star. Squares show the mean progenitor mass in 0.2 dex bins, while the error bars show the scatter in the mean mass. Lower mass SN progenitors enter later, with the  $8 - 12 M_{\odot}$  stars that probably give rise to the r-process elements entering at  $[\text{Fe}/\text{H}] \sim -3$ . Panel D: As a function of final stellar metallicity, the number of SN progenitors. For a given  $[\text{Fe}/\text{H}]$ , the number of progenitors can show a wide scatter. The mean number of progenitors is 10 at roughly  $[\text{Fe}/\text{H}] = -2.8$ .

lution in the galaxy. With  $> 10^5$  stars these surveys could move the  $F_0$  constraint near or past the  $F_0 \sim 10^{-4}$  contour in Figure 6, or even find a true Population III star. Their real power may lie in their ability to provide enough data for individual SNe yields to be extracted empirically. If one of these surveys does manage to discover a true metal-free star, it will be very interesting in its own right. If no truly metal-free old stars are found in these expanded samples, they will tighten the constraint on  $F_0$  and force the first-stars IMF to even more skewed high masses.

By obtaining colors, radial velocities, and metallicities for large samples of Galactic halo stars, these surveys hope to achieve “chemical tagging”, or the identification of distinct groups of kinematically and chemically related stars that would arise from a single coherent formation history. This result would constitute a major achievement in “near-field cosmology” (Freeman & Bland-Hawthorn 2002). Even if they succeed, these ambitious efforts will boost, and not moot, theoretical efforts like the one reported here. These surveys can provide additional known and reliable laboratories to

study detailed chemical evolution, where we now operate on sample of indistinguishable stars without regard to their individual kinematic histories and no reliable way to group them except by metallicity. At the same time this observational technique will provide critical information on the CDM history of the Galaxy, such that a detailed actual history may some day be constructed with a combination of theory and data. There will still be ample room for theory to reconstruct the possible chemical histories and relate them to other indicators, and connect them to the “cosmology” in “near-field cosmology”, with a new level of rigor and accuracy. As stated before, this theoretical study is only the beginning step in this long process.

The real power of this chemical evolution model to constrain reionization will come when it is applied to a wide range of halo masses and redshifts, so that various reionization histories and chemical evolution trajectories can be related in detail for full galaxy populations. This effort will be reported in a later paper.

My results also point to an important lesson about the power of theoretical calculations of supernova yields to

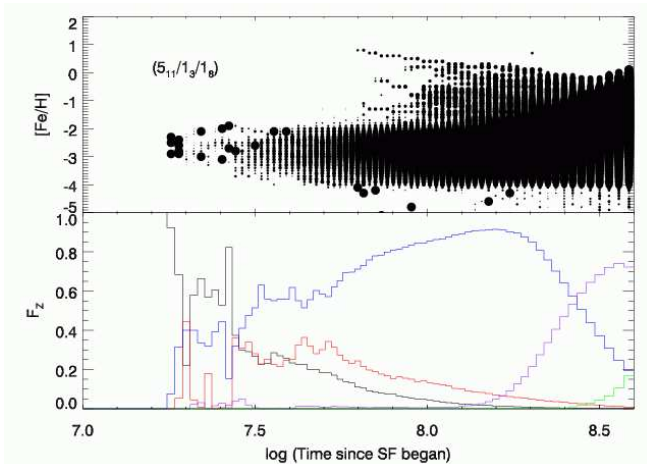


FIG. 11.— Upper panel: The distribution of stellar metallicities and birth times for the fiducial (5<sub>11</sub>/1<sub>3</sub>/1<sub>8</sub>) tree and IMF case A, showing the spread in times for a single [Fe/H], or the spread in [Fe/H] at a given time. The symbol sizes are proportional to the number of stars in each event. Clearly time and metallicity are not perfectly correlated. For instance, stars with [Fe/H] = -3 form over a period of 500 Myr. Lower panel: The fraction of stars in different metallicity ranges, as a function of time since the onset of star formation. Stars with [Fe/H] < -4 in black, -4 ≤ [Fe/H] ≤ -3 in red, -3 ≤ [Fe/H] ≤ -2 in blue, -2 ≤ [Fe/H] ≤ -1 in purple, and ≤ -1 [Fe/H] ≤ 0 in green. Star formation is essentially all metal free for ~ 10<sup>7</sup> yr, and down to ~ 20% of the total by 30 Myr.

constrain the mass function of the first stars. As shown in § 5, the yields of PISNe are difficult to completely rule out based on comparisons of theoretical yields directly to the data. This difficulty is represented here by the constraints offered by [Zn/Fe] and the difficulty of pushing it any further. By comparison with the robust constraint on the strong VMS hypothesis offered by the r-process elements, the argument based on [Zn/Fe] seems crude. This point illustrates the importance of identifying clean signatures for particular mass ranges of the IMF. If, for instance, the r-process is isolated to the 8 - 12  $M_{\odot}$  for low-metallicity stars, the constraints on the upper end of the IMF can be improved. Where possible, theorists should attempt to isolate such clear indicators of stellar mass in their increasingly sophisticated models.

## 8. CONCLUSIONS

I have presented a new treatment of chemical evolution in the earliest phases of Galaxy formation. This model is motivated by and integrated with the theory of hierarchical galaxy formation. As a result, this model can be formally connected to high-redshift star formation, allowing detailed connections between disparate phenomena. This simple model can reproduce the main properties of the Galactic halo metallicity distribution as well or better than classical theories of chemical evolution (see Oey 2002 and Qian and Wasserburg 2002 for recent examples), which cannot be formally connected to high-redshift data in such detail. The basic structure of the model follows chemical evolution of stars and star-forming gas within dark matter halos whose masses are specified by the hierarchical theory of structure formation and which merge and evolve according to a well-known framework. Within each halo, the treatment of chemical evolution is more akin to standard the-

ory, but with some improvements, mainly related to the stochastic treatment of early star formation. The model advances the interpretation of metal-poor stars in the Galaxy by generating detailed chemical evolution histories for each metal-poor star in the model. Most importantly, this model allows *quantitative* hypothesis testing of novel theoretical ideas that have been lacking in material connection to the available data. This new framework is simple, flexible, and fast, so that almost any new idea about early stellar and interstellar evolution can be readily incorporated and connected to the whole of the present and future data.

Based on the hundreds of individual models run with this new framework, and the best available data, I draw the following key conclusions:

1. The non-detection of true Population III stars in the Galactic halo strongly suggests that there is some critical metallicity,  $Z_{crit} \lesssim 10^{-4}$ , below which low-mass star formation was inhibited. The precise value of  $Z_{crit}$  cannot be determined within the range  $0 < Z_{crit} \lesssim -4$  because the Galactic MDF has not yet shown a statistically significant deficit of low-[Fe/H] stars (except for true Population III).
2. The frequency of true Population III stars,  $F_0$ , is robust indicator of the IMF below  $Z_{crit}$  because variations in model parameters for halo formation and mixing are overwhelmed by changes in the IMF. The IMFs that best fit all the available data from metal-poor stars and reionization have log-normal parameters  $m_c = 6 - 35 M_{\odot}$  and  $\sigma = 0.3 - 1.2$ , and mean masses  $\langle M \rangle = 8 - 42 M_{\odot}$ . These masses are close to the predictions from theoretical models of primordial star formation that include formation feedback.
3. For a given set of parameters, individual chemical evolution histories can be calculated for each model metal-poor star. Population II stars with [Fe/H] ≤ -3 (EMPs and below) have 1 - 10 metal-free SN progenitors, suggesting that the trends in EMP ratios such as [Zn/Fe] result from variations in the masses of precursor SNe. This result is a significant advance in comparing detailed yields of the first SNe to theoretical calculations.

With the advent of new large telescopes devoted to high-redshift studies of galaxies, and large surveys of metal-poor stars in the Milky Way and other galaxies, we are entering a new age of rich information about early star formation and chemical enrichment. This study is the first step in a large effort to use the tools of theory to relate different types of observation together. As these issues develop, the new theoretical framework developed here will be extended and improved to analyze new information in unified, coherent way. It may turn out that the history of cosmic star formation is written in the Galaxy. Only by combining all of the state-of-the-art data can we be sure of confidently reaching detailed conclusions about the first stars in the universe.

This work would not have been possible without the generous support of the Department of Astronomy and

TABLE 2  
MODEL CONSTRAINTS

Datum	Value	Constraint
Galactic Halo MDF	shape	disk/halo separation, IMF
Population III fraction, $F_0$	$\leq 0.0019$	Lower end of IMF
Ionizing efficiency $\gamma_0$	$\geq 34000$	Lower end of IMF
Maximum $[Zn/Fe]$ , 8 - 40 $M_\odot$	$\leq 1.0$	Upper end of IMF
$F_{VMS}$ , VMS iron budget	$\leq 0.5$	Upper end of IMF
Fraction of r-process enriched stars	$\geq 0.82$	Upper end of IMF

Astrophysics at the University of Chicago. It is my pleasure to acknowledge Jim Truran, Joss Bland-Hawthorn, and Vikram Dwarkadas for interesting and helpful conversations, and Tim Beers for these and detailed comments on the manuscript. This study grew out of ongoing

work with my valued collaborators Aparna Venkatesan and Mike Shull, and I am grateful for their continuing stimulation and encouragement, and for comments on the manuscript.

#### APPENDIX

This appendix discusses the many details involved in the halo merger tree model. Most of the extended Press-Schechter formalism relies on the expression for the variance of the initial Gaussian random density field, expressed in Fourier  $k$ -space:

$$S(M) \equiv \sigma^2(M) = \frac{1}{2\pi^2} \int_0^\infty k^2 P(k) \bar{W}^2(kR) dk \quad (1)$$

In theory the integral is over the full range  $k = 0 - \infty$ , but in practice the range is considered to be  $k = 0.001 - 1000 \text{ Mpc}^{-1}$ . In this relation,  $P(k)$  is the matter power spectrum:

$$P(k) = \xi k^n T^2(k). \quad (2)$$

Assuming  $n = 1$  and the transfer function  $T(k)$  derived by Bardeen et al. (1986),

$$T(k) = \frac{\ln(1 + 2.34q)}{2.34q} [1 + 3.89q + (16.1q)^2 + (5.46q)^3 + (6.71q)^4]^{-1/4}, \quad (3)$$

where  $q = k/(\Omega_M h^2 \text{Mpc}^{-1})$ . In Equation (A1), the Fourier transform of the top-hat filtering function is given by:

$$\bar{W} = \frac{3}{(kR)^3} [\sin(kR) - (kR) \cos(kR)] \quad (4)$$

Finally, the normalization constant  $\xi$  is found by evaluating the integral (A1) and equating the result to  $\sigma_8^2$ , the variance over spheres of  $R = 8h^{-1} \text{ Mpc}$ . The linear growth function from Carroll, Press, & Turner (1992) extrapolates the linear density field to the present day:

$$D(z) = \frac{g(z)}{g(0)(1+z)} \quad (5)$$

where

$$g(z) = \frac{5}{2} \Omega_M \left[ \Omega_M^{4/7} - \Omega_\Lambda + \left( 1 + \frac{\Omega_M}{2} \right) \left( 1 + \frac{\Omega_\Lambda}{70} \right) \right]^{-1} \quad (6)$$

With all these pieces in place, the Press-Schechter function describing the number density of dark matter halos of between mass  $M$  and  $M + dM$  is:

$$ndM = \sqrt{\frac{2}{\pi}} \frac{\bar{\rho}}{M} \frac{\delta_c(z)}{\sigma^2(M)} \exp \left[ -\frac{\delta_c^2(z)}{2\sigma^2(M)} \right] dM \quad (7)$$

In this expression,  $\delta_c(z)$  is the redshift-dependent critical overdensity for collapse,  $\delta_c(z) = \delta_{c,0}/D(z)$  and  $\delta_{c,0} = 1.686$ .

#### REFERENCES

- Abel, T., Bryan, G. L., & Norman, M. L. 2002, *Science*, 295, 93  
 Adams, F. C., & Laughlin, G. 1996, *ApJ*, 468, 586  
 Aguirre, A., Hernquist, L., Schaye, J., Katz, N., Weinberg, D. H., & Gardner, J. 2001, *ApJ*, 561, 521  
 Baade, W. 1944, *ApJ*, 100, 137  
 Bardeen, J. M., Bond, J. R., Kaiser, N., & Szalay, A. S. 1986, *ApJ*, 304, 15  
 Barklem, P., et al. 2005, *A&A*, in press  
 Beers, T. C., Preston, G. W., & Schechtman, S. A. 1992, *AJ*, 103, 1987  
 Beers, T. C. 2005 private communication

- Beers, T. C., & Christlieb, N., 2005, *ARA&A*, in press
- Bromm, V., Coppi, P., & Larson, R. B. 2001, *MNRAS*, 328, 969
- Bromm, V., & Loeb, A. 2002, *NewA*, 9, 353
- Bromm, V., & Loeb, A. 2004, *Nature*, 425, 812
- Bromm, V. & Larson, R. B. 2004, *ARA&A*, 42, 79
- Burris, D., et al. 2000, *ApJ*, 544, 203
- Carney, B. W., Laird, J. B., Latham, D. W., & Aguilar, L. A. 1996, *AJ*, 112, 668
- Carretta, E., Gratton, R., Cohen, J.G., Beers, T. C., & Christlieb, N. 2002, *AJ*, 124, 481
- Carroll, S. M., Press, W. H., & Turner, E. L. 1992, *ARA&A*, 30, 499
- Cen, R. 2003, *ApJ*, 591, L5
- Ciardi, B., Ferrara, A., & White, S. D. M. 2003, *MNRAS*, 344, 7
- Christlieb, N., et al. 2003, *Nature*, 419, 904
- Cayrel, R., et al. 2004, *A&A*, 416, 1117
- Cohen, J. G., et al. 2004, *ApJ*, 612, 1107
- Fields, B. D., Truran, J. W., & Cowan, J. J. 2002, *ApJ*, 575, 845
- Figer, D. 2005, *Nature*, 434, 192
- Frebel, A., et al. 2005, *Nature*, 434, 871
- Freeman, K. C., & Bland-Hawthorn, J. 2002, *ARA&A*, 40, 487
- Gnedin, N. 1998, *MNRAS*, 294, 407
- Haiman, Z., & Loeb, A. 1997, *ApJ*, 483, 21
- Haiman, Z., & Holder, G. P. 2003, 595, 1
- Heger, A., & Woosley, S. 2002, *ApJ*, 567, 532 (HW02)
- Kitayama, T., Yoshida, N., Susa, H., & Umemura, M. 2004, *ApJ*, 613, 631
- Lacey, C., & Cole, S. 1993, *MNRAS*, 262, 627 (LC93)
- Larson, R. B. 1973, *MNRAS*, 161, 133
- Leitherer et al., 1999, *ApJS*, 123, 3
- Liddle, A. R., & Lyth, D. H. 2000, *Cosmological Inflation and Large-Scale Structure* (Cambridge: Cambridge Univ. Press)
- Loeb, A., & Barkana, R. 2001, *ARA&A*, 39, 19
- Lucatello, S., Gratton, R. G., Beers, T. C., Carretta, E. 2005, *ApJ*, in press
- Madau, P., Ferrara, A., & Rees, M. J. 2001, *ApJ*, 555, 92
- Malhotra, S., Rhoads, J. E. 2002, *ApJ*, 565, L71
- McWilliam, A., Preston, G. W., Sneden, C., & Searle, L. 1995, *AJ*, 109, 2757
- Mo, H. J., & White, S. D. M. 2002, *MNRAS*, 336, 112
- Oey, M. S. 2000, *ApJ*, 542, L25
- Oey, M. S. 2002, *MNRAS*, 339, 849
- Omukai, K., & Palla, F. 2002, *ApJ*, 589, 677
- Omukai, K., Tsuribe, T., Schneider, R., & Ferrara, A. 2005, *ApJ*, 626, 627
- Press, W. H., & Schechter, P. 1974, *ApJ*, 187, 425
- Qian, Y.-Z., & Wasserburg, G. J. 2002, *ApJ*, 567, 515
- Ryan, S. G., & Norris, J. E. 1991, *AJ*, 101, 1865 (RN91)
- Salpeter, E. E. 1955, *ApJ*, 121, 161
- Santoro, F., & Shull, J. M. 2005, *ApJ*, in preparation
- Scannapieco, E., Schneider, R., & Ferrara, A. 2003, *ApJ*, 589, 35
- Schaerer, D. 2002, *A&A*, 382, 28
- Schaye, J., Aguirre, A., Kim, T. S., Theuns, T., Rauch, M., & Sargent, W. L. W. 2003, *ApJ*, 596, 768
- Schneider, R., Ferrara, A., Natarajan, P., & Omukai, K. 2002, *ApJ*, 571, 30
- Somerville, R. S., & Kolatt, T. S. 1999, *MNRAS*, 305, 1 (SK99)
- Somerville, R. S., & Primack, J. R. 1999, *MNRAS*, 310, 1087
- Spergel, D. N., et al. 2003, *ApJS*, 148, 175
- Spitzer, L. 1978, *Physical Processes in the Interstellar Medium*, (New York: Wiley)
- Tan, J., & McKee, C. M. 2002, in “The Emergence of Cosmic Structure”, *Proceedings of the AIP*, 666, 93
- Tan, J., & McKee, C. M. 2004, *ApJ*, 603, 683
- Truran, J. W., Cowan, J. J., Pilachowski, C. A., & Sneden, C. 2002, *PASP*, 114, 1293
- Tumlinson, J., & Shull, J. M. 2000, *ApJ*, 528, L65
- Tumlinson, J., Giroux, M. L., & Shull, J. M. 2001, *ApJ*, 550, L1
- Tumlinson, J., Venkatesan, A., & Shull, J. M. 2004, *ApJ*, 612, 602 (TVS04)
- Tumlinson, J., Shull, J. M., & Venkatesan, A. 2003, *ApJ*, 584, 608 (TSV03)
- Umeda, H., & Nomoto, K. 2005, *ApJ*, 619, 427
- Venkatesan, A., Tumlinson, J., & Shull, J. M. 2003, *ApJ*, 584, 621
- Woosley, S. E., et al. 1994, *ApJ*, 433, 229
- Woosley, S. E., & Weaver, T. A. 1995, *ApJS*, 101, 181